CHAPTER 3

THE LANAWAY FIELD CASE STUDY

On the basis of conventional surface seismic data, an exploratory well (referred to as the VSP well in this chapter) was drilled in 1986 into the up-dip, raised rim of the Devonian Leduc Formation reef complex at Lanaway Field, southwestern Alberta, Canada. The stratigraphy of the Central Plains of the Western Canadian Sedimentary Basin is listed in Figures 3.1A, B, and C (representing the stratigraphic sequence from the Quaternary to the Cambrian Periods) .

The VSP well was expected to encounter an anomalous late-stage carbonate accretionary buildup at the Leduc level. It was anticipated that the Leduc at the VSP well location would be up to 80 m higher than at adjacent rim well sites. The envisioned accretionary growth was not present; the top of the Leduc in the VSP well was consistent with other rim wells along the Lanaway/Garrington reef trend (Fig. 3.2) and inconsistent with the seismic interpretation (Hinds et al., 1989a, Hinds et al., 1994a and 1994c). Fortunately, however, the Leduc was structurally closed and the VSP well was completed as an oil well (producing both from the Nisku and Leduc Formations).

In order to resolve the apparent discrepancy between the interpreted surface seismic data and geology at the VSP well, a near offset vertical seismic profile (VSP) was conducted at the

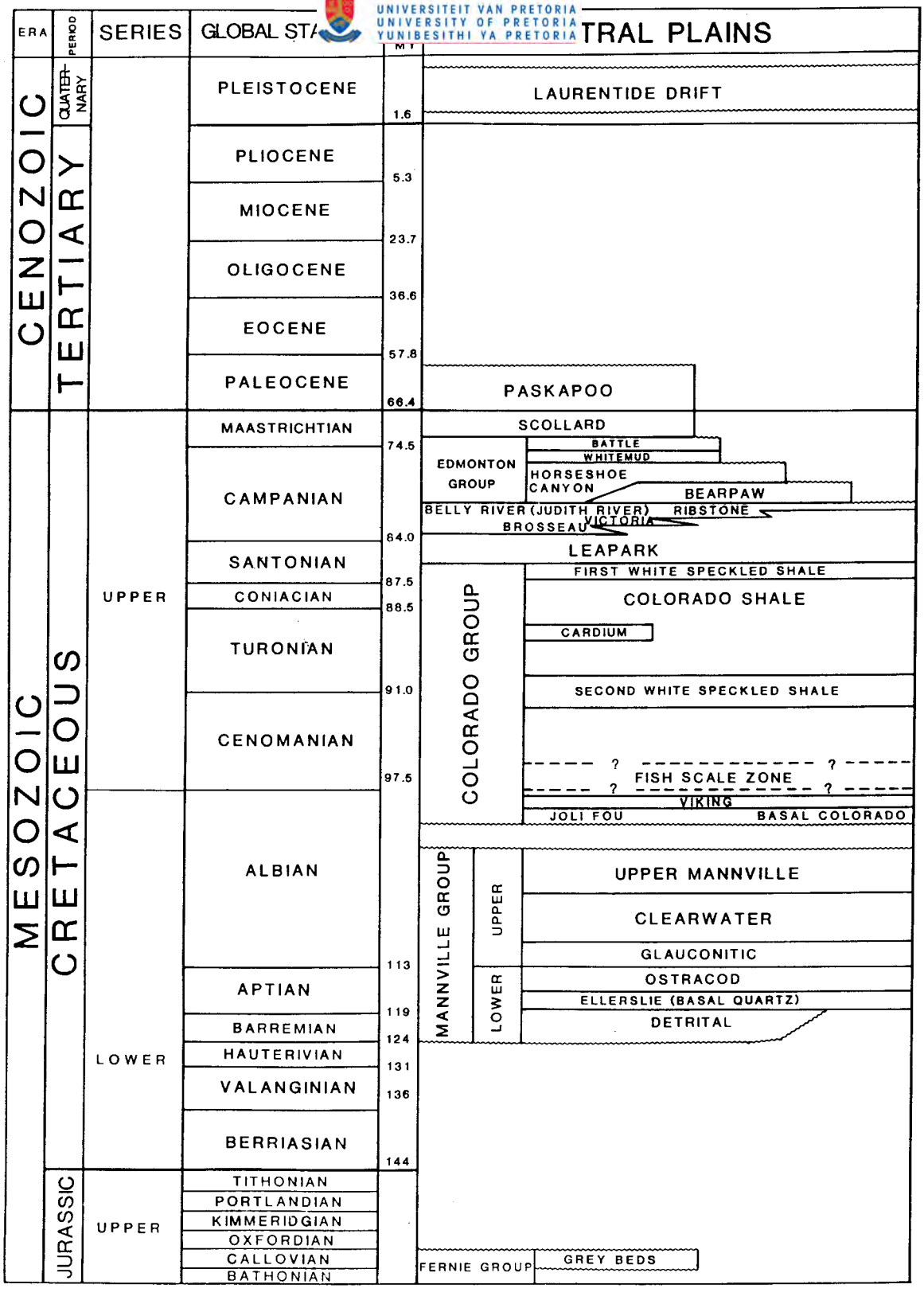

Figure 3.1A Stratigraphy from the Quaternary (Cenozoic) to the Upper Jurassic (Mesozoic) periods of the Central Plains area of the Western Canada Sedimentary Basin (after AGAT Laboratories, 1988; Anderson et al., 1989d; Hinds et al., 1994a and c)

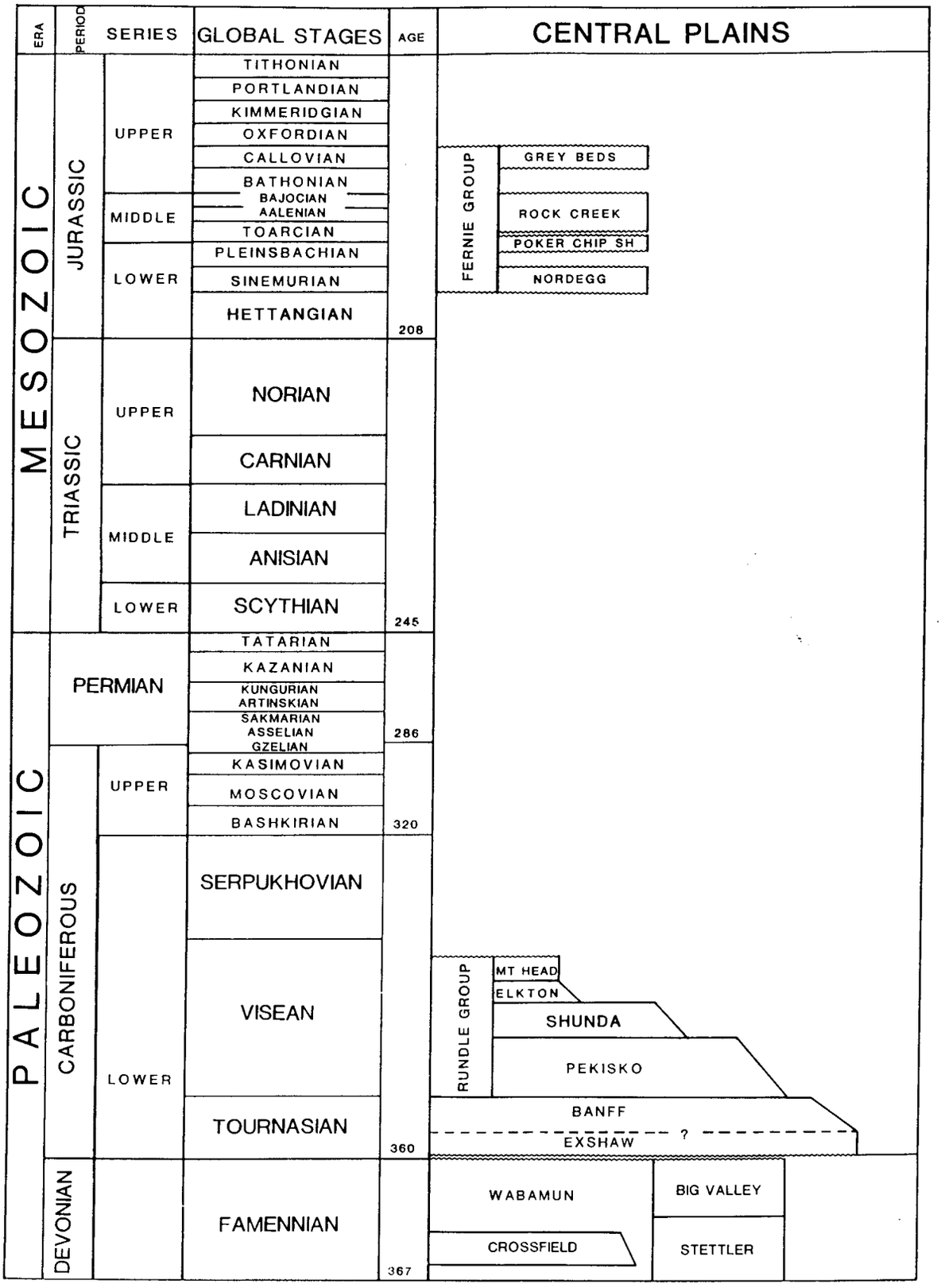

Figure 3.1B Stratigraphy from the Upper Jurassic (Mesozoic) to the Upper Devonian (Paleozoic) periods of the Central Plains area of the Western Canada Sedimentary Basin (after AGAT Laboratories, 1988; Anderson et al., 1989d; Hinds et al., 1994a and c)

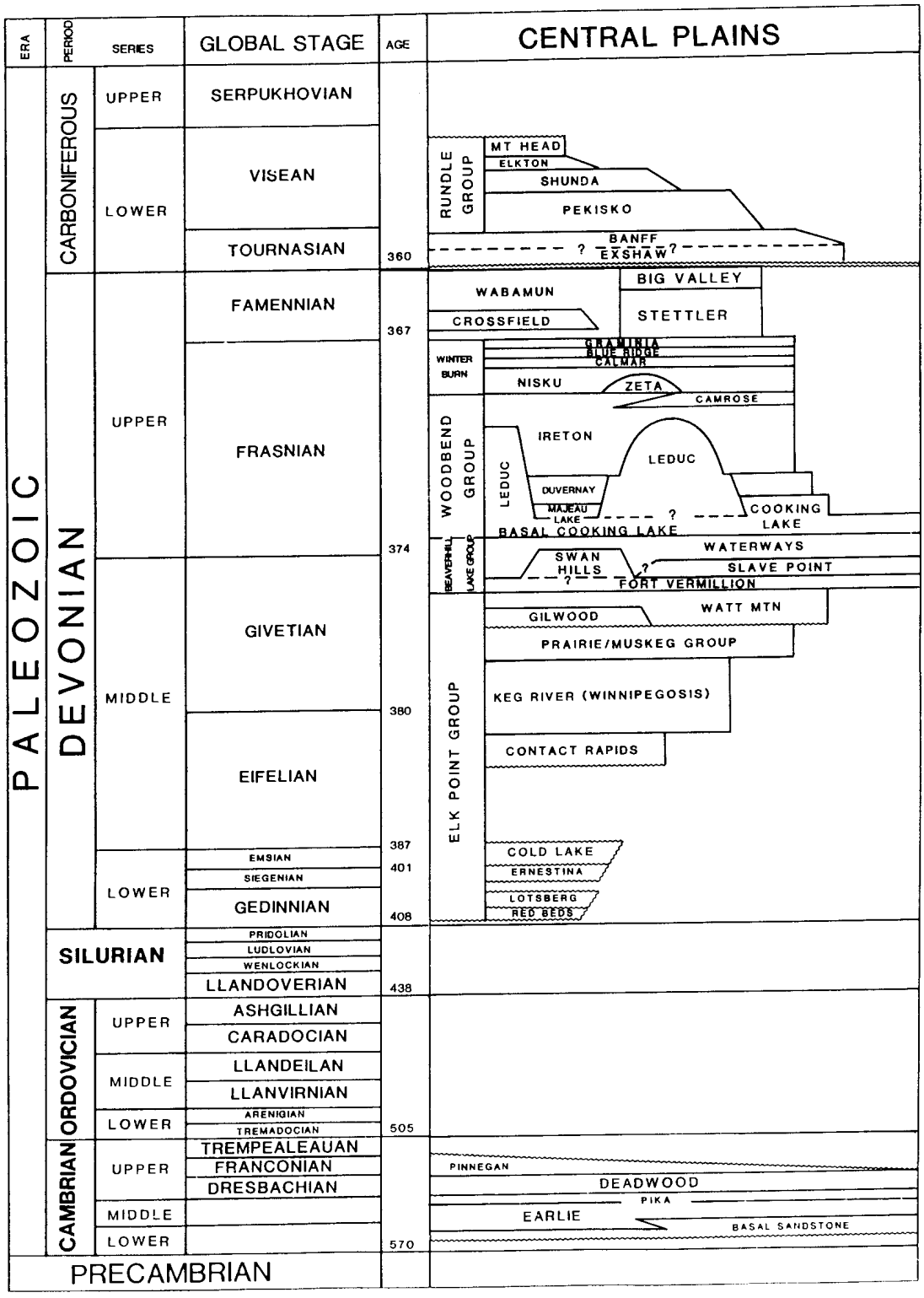

Figure 3.1C Stratigraphy from the Upper Carboniferous (Paleozoic) period to the Precambrian of the Central Plains area of Western Canada Sedimentary Basin (after AGAT Laboratories, 1988; Anderson et al., 1989d; and Hinds et al., 1994a and c)

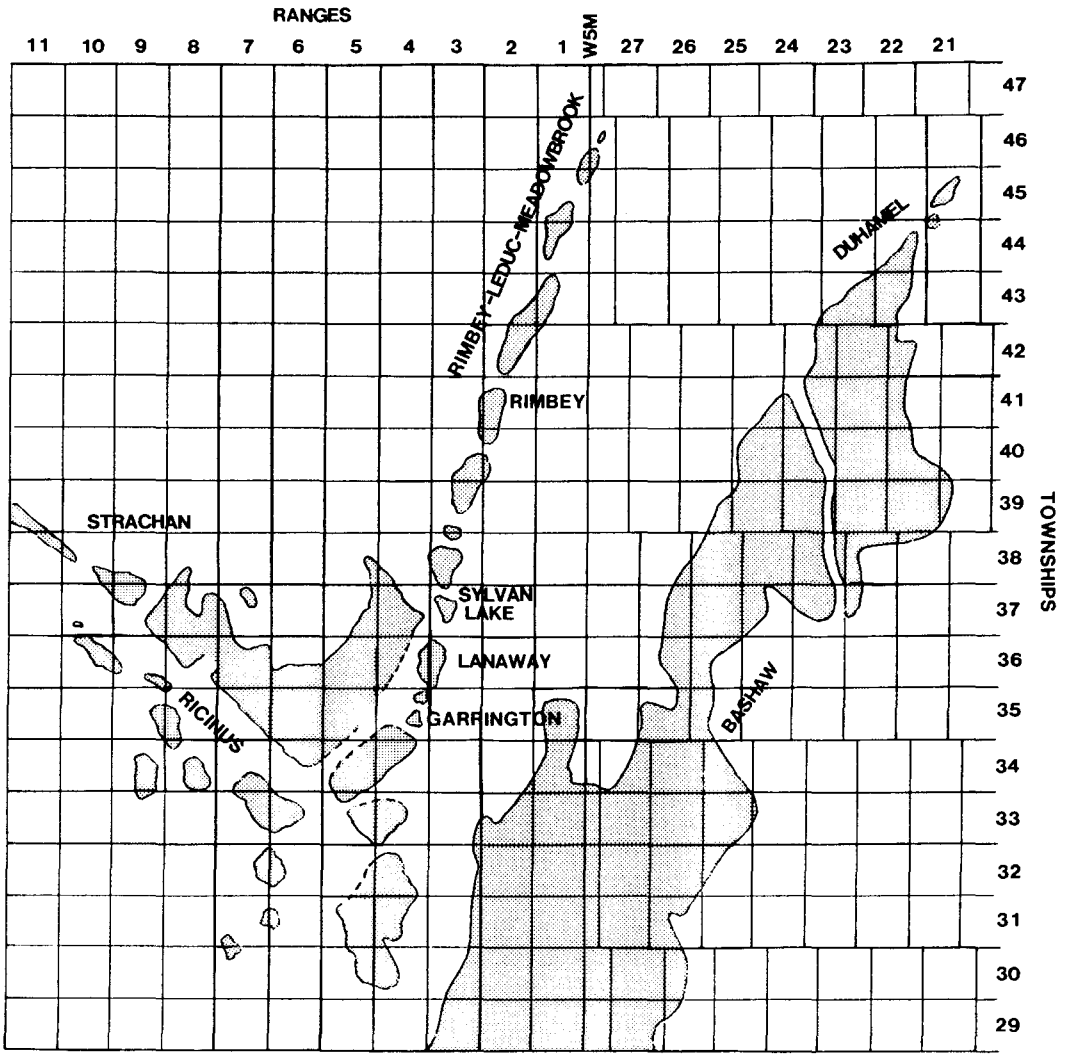

Figure 3.2 Regional location map of the Lanaway study area. The shaded areas represent the areal extent of the major Leduc Formation carbonate reefs of the area (with permission of Talisman Resources Inc.; from Hinds et al., 1994a and c)

well site. The interpretation of the VSP was expected to elucidate the geological origin of the misinterpreted seismic anomaly. Towards this end, the interpretation of the VSP was relatively successful in being able to assist in the formulation of an explanation for the anomaly. These data confirmed that the original interpretation of the surface seismic data (with respect to the Nisku, Ireton and Leduc top) was incorrect, and that the anomaly observed on the surface seismic line was not a processing artifact. The anomaly could most probably be attributed to either 1) structural relief at the pre-Cretaceous subcrop (as exemplified by Shunda Formation isopach values); 2) stratigraphic anomalies (thicker sections of carbonates) within the Winterburn Group or 3) seismic focusing caused by draping Ireton over the nose of the reef along the traverse of the seismic line. Interbed multiples interfering with the Nisku event could possibly be a minor contributing factor.

3.1 Carbonate reef development in the Western Canadian Sedimentary Basin

As an introduction to the geology of the carbonate reef case studies presented in this chapter (Lanaway Field), chapter 4 (Ricinus Field) and chapter 6 (Simonette Field), the depositional sequence history will be reviewed below for the Hume-Dawson to the Beaverhill-Saskatchewan subsequences (Moore, 1988 and 1989a) in the Western Canadian Sedimentary Basin (WCSB).

The case studies pertain to the Leduc reefs of the Saskatchewan Group subsequence (Moore, 1988). There are three major subsequences which involve oil producing carbonate reefs; namely the Upper Keg River, Rainbow and Upper Winnipegosis reefs of the Hume-Dawson subsequence, the Swan Hills Fm reefs of the Beaverhill subsequence and the Leduc Fm reefs

of the Saskatchewan subsequence. The Devonian history of the WCSB is divided into five major rock sequences; each divided by discontinuities that encompass a period of sea-level rise followed by a fall of sea level and ending in emergence (Moore, 1988). The reef building is pulsatory resulting in the different subsequences.

The first rise of sea level in these reef-building subsequences (Hume-Dawson) occurred during the deposition of the Lower Keg River Member in Northern Alberta and the Lower Winnipegosis unit in Southern Saskatchewan (Brown et al., 1990). As shown in Moore (1988), the Keg River barrier reef (or Keg River - Pine Point barrier reef; Moore, 1989a) formed northeastward of the Peace River Arch. Behind this barrier reef, pinnacles up to 200 m in height grew in the Keg River and Winnipegosis Fms within the Elk Point Basin (see Fig. 5 of Moore, 1988). Transgression at the end of Winnipegosis/Keg River time resulted in basin shallowing and reef growth termination within the resulting hypersaline environment. The basal salt units of the Prairie Fm and the Black Creek Member of the Muskeg Fm were deposited during this time of limited water circulation within the Elk Point Basin. The end of the sequence resulted in further deposition of anhydrites, shales and carbonates followed by the Watt Mountain unconformity. Anderson et al. (1989d) shows examples of Elk Point carbonate reservoir seismic signatures.

The next two subsequences correspond to the Beaverhill Gp (late Givetian to early Frasnian) and the Saskatchewan Gp (mid-Frasnian to end of Frasnian). The depositional history of both of these subsequences contain a carbonate platform development, platform reef growth, basin filling by mixed carbonates and siliciclastics and finally, by progradation of the carbonate platforms (Moore, 1989a).

The Beaverhill Gp subsequence contained the Swan Hills Formation reefs, the Waterways Formation shales and finally the Cooking Lake Formation carbonate platform. The Swan Hills reefs are seismically described in Anderson et al. (1989a) and Ferry (1989). The growth of the Swan Hills reefs was mostly pulsatory and the reefs have been categorized into several cycles of reef "layering" (Wendte and Stoakes, 1982). The progradation of the carbonate platform at the end of the subsequence resulted in the deposition of the lower part of the Cooking Lake Fm. The Peace River Arch was still a positive feature at this time (Chapter 5).

The carbonate platform of the reefs of the Saskatchewan subsequence is either the Cooking Lake Fm or an argillaceous ramp of the Waterways Formation. The Leduc reefs have been divided into three geographical realms in Stoakes and Wendte (1987). The Leduc platform reefs in the southeastern realm include the Bashaw-Duhamel and Rimbey-Meadowbrook reef chains, Ricinus Field and Lanaway Field. These reefs have the Cooking Lake Fm as a platform facies. The reefs of the western region such as the Simonette Field (Chapter 6) are built on the Waterways Fm. The northwestern realm reefs generally fringe the Peace River Arch. Anderson et al. (1989c) shows examples of Woodbend Group reef seismic signatures.

Nisku Fm (Upper Frasnian) reefing occurred in the West Pembina Shale Basin. The reefing in the Nisku Fm may be Zeta Lake member pinnacles or carbonate porosity resulting from drape over the larger Leduc reefs (as in Chapter 3). The basin infill period saw the deposition of the Nisku Fm and Birdbear Fm platform carbonates. The end of the Frasnian is highlighted by an extinction event which may be due to a meteorite impact (Moore, 1988).

3.1.1 Lanaway Field

The Upper Devonian Woodbend Group in central Alberta is subdivided into four formations: Cooking Lake, Duvernay, Leduc, and Ireton. The Cooking Lake represents platform facies. The Leduc is reefal facies; the Duvernay and Ireton are inter-reef shales (Anderson et al., 1989a, b and c; Klovan, 1964; McNamara and Wardlaw, 1991; Moore, 1988, 1989a and b; Mossop, 1972; Mountjoy, 1980; Stoakes, 1980; Stoakes and Wendte, 1987; and Hinds et al., 1994a).

The Leduc Formation at Lanaway (Figs. 3.2 and 3.3) is interpreted to be a large atoll. It towers some 200 m above the Cooking Lake platform and exhibits a seismically mappable (peripheral) raised rim and a structurally lower central lagoonal area. Such raised rims are described in Mossop (1972) in his study of the isolated Leduc Formation limestone reef complex at Redwater. In that study the raised rim was postulated to arise primarily as a result of the greater degree of differential compaction of the central lagoonal facies in comparison to the rigid reef facies. The updip edge (to the northeast) of the raised rim at Lanaway is productive where the reef is structurally closed and effectively sealed by the inter-reef shales of the Duvernay and Ireton Formations (Hinds et al., 1994a). The geologic cross-sections shown in Figures 3.4, 3.5 and 3.6 (from wells shown in Fig. 3.3) and the seismic section (Fig. 3.7, on the seismic line on Fig. 3.3) illustrate the interpreted morphological relationships between the Leduc and inter-reef shales of the Ireton and Duvernay in the Lanaway area.

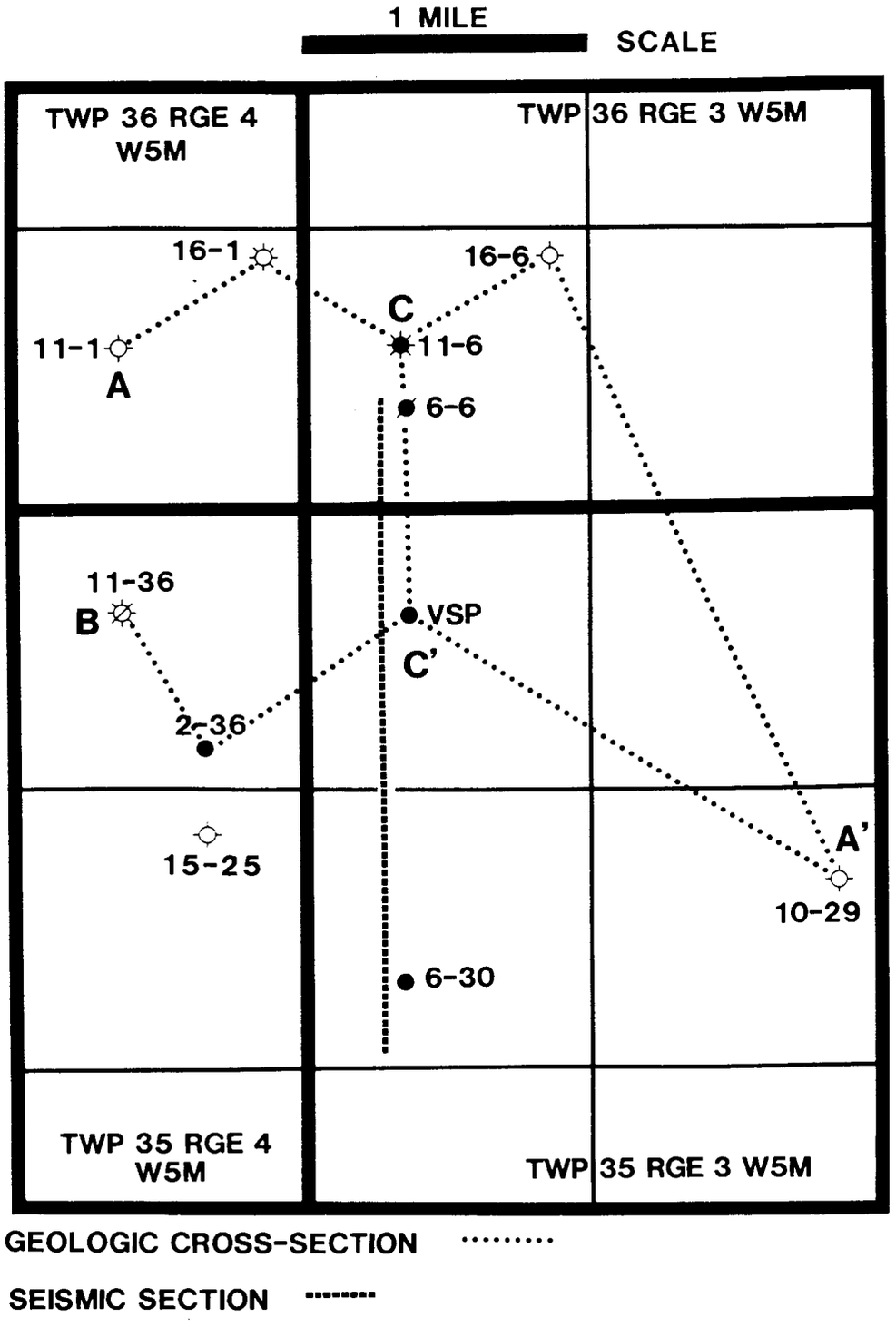

Figure 3.3 Detailed map of the Lanaway study area displaying the seismic section traverse for the seismic data shown in Figures 3.7, 3.8, 3.14 and 3.15 and the locations of the wells used in the geological cross-sections shown in Figures 3.4, 3.5 and 3.6 (from Hinds et al., 1994a and c).

On the surface seismic data, the Lanaway Leduc reef is readily differentiated from inter-reef shales. The carbonate build-up is characterized by appreciable velocity pull-up (25 ms), time-structural drape at the top of the Devonian (25 ms) and character variations within the Woodbend Group (associated with the abrupt transition from shale to reefal facies). Back from the steeply dipping edge, the top of the reef is clearly defined on seismic data, being manifested as a high-amplitude peak on normal polarity data.

The results and interpretations of the 2-D surface seismic and VSP surveys (performed on well C' shown in Fig. 3.3) and the seismic signatures of the top of the Leduc reef at Lanaway are discussed in this chapter. The seismic data were acquired prior to drilling the VSP well, which ultimately ended up intersecting the reef some 80 m below the prognosed depth while the VSP survey was run in an attempt to resolve the apparent discrepancy between the interpreted depth of the reef as derived from surface seismic data and the geology at the exploratory (VSP) well.

3.2 Well Nomenclature

The nomenclature for well locations within the Western Canadian Sedimentary Basin (WCSB) generally comprises a four number reference system (Anderson et al., 1989b). The two numbers (as in the well location 11-1 in Fig. 3.3) are a short form for a more detailed well location system utilized within the WCSB area. The well location system will be described briefly in order to assist the reading of the maps in this and later chapters.

As seen in Figures 3.2 and 3.3, geographical areal units are used in the WCSB referred to as Townships and Ranges. Townships increase in value from South to North and Ranges increase in value (until a Meridian is crossed) from East to West. A single Township and Range involve an area of six by six miles. The Township and Range square is subdivided into thirty-six square units called Sections. Each Section is one mile by one mile in size and is numbered 1 to 36, starting in the southeast corner of the Township and Range square. The smallest sub-division is the land survey division (LSD) which is a quarter mile by quarter mile in size. Within each section, there are sixteen quarter-section LSD's. The LSD numbering starts in the southeast corner of the section. The Ranges are referenced to Meridian lines (lines accurately running north and south through any point on the Earth's surface). After a major Meridian line is crossed, the Range values restart at 1.

As seen in Figure 3.2, the Lanaway Field lies within Ranges 3 and 4 and Township 36 and is west of the fifth Meridian (labelled W5M in Figure 3.2). In Figure 3.3, the two digit well name refers to the LSD and Section numbers. The well 11-1 lies in the 11th LSD of Section 1. The well is geographically tied to the quarter by quarter mile land spacing unit. The full name of the well would be 11-1-36-4 W5M (LSD-Section-Township-Range). For this and the other chapters concerning the case studies, the well name can, at times, be shown in the shortened format as in the example of 11-1.

3.3 Lanaway Field (at the VSP well)

Full Leduc reef at Lanaway Field towers up to 200 m above the Cooking Lake platform and has a structurally lower interior lagoon (Figs. 3.4 and 3.5). Production from the Leduc is

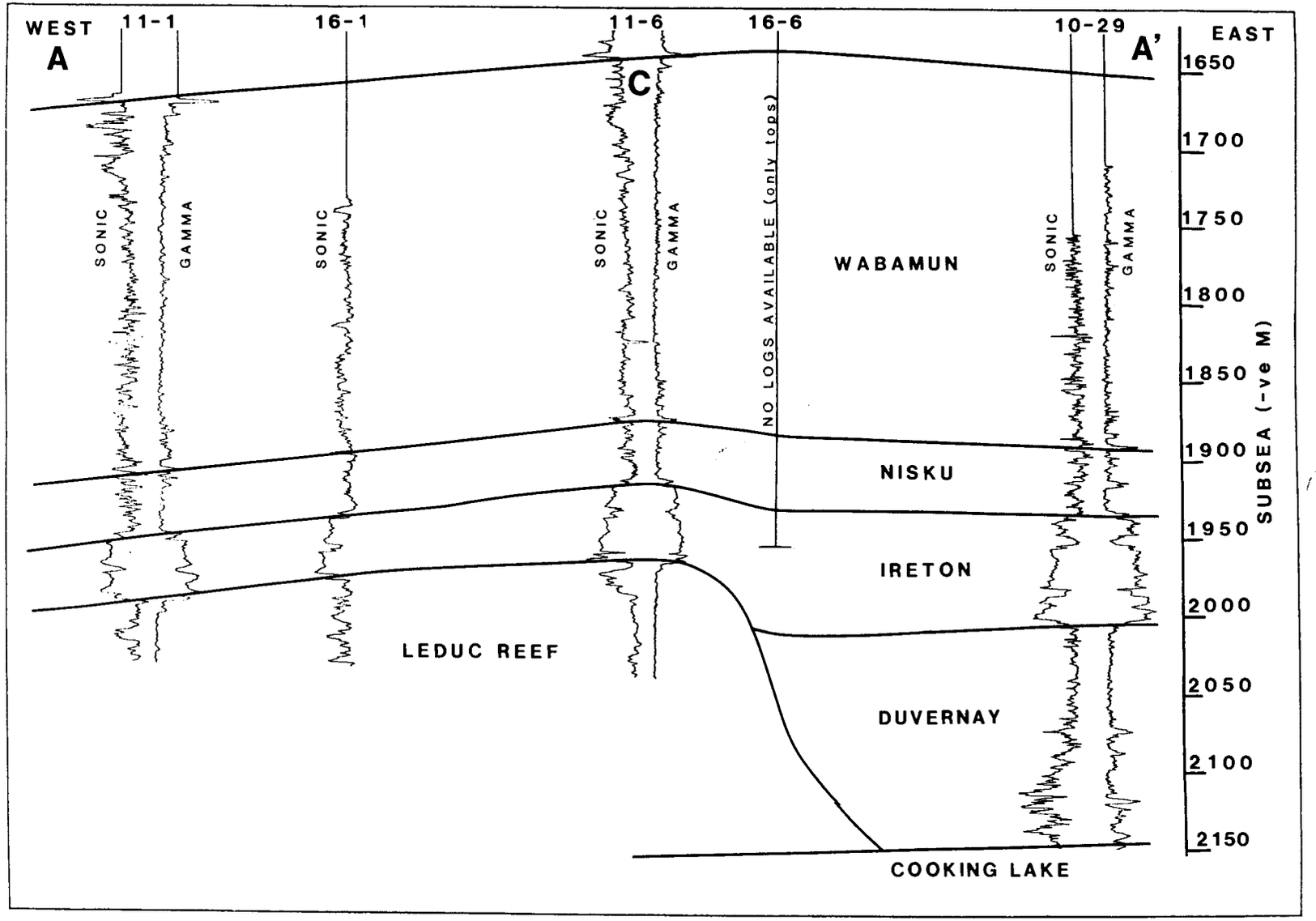

Figure 3.4 West-east geologic cross-section A-A' (refer to Figure 3.3 for well locations). The Leduc Formation reef in well 11-1 is structurally low and wet; wells 16-1 and 11-6 are productive (Leduc oil reservoirs); and wells 16-6 and 10-29 are off-reef and abandoned (from Hinds et al., 1994a and c).

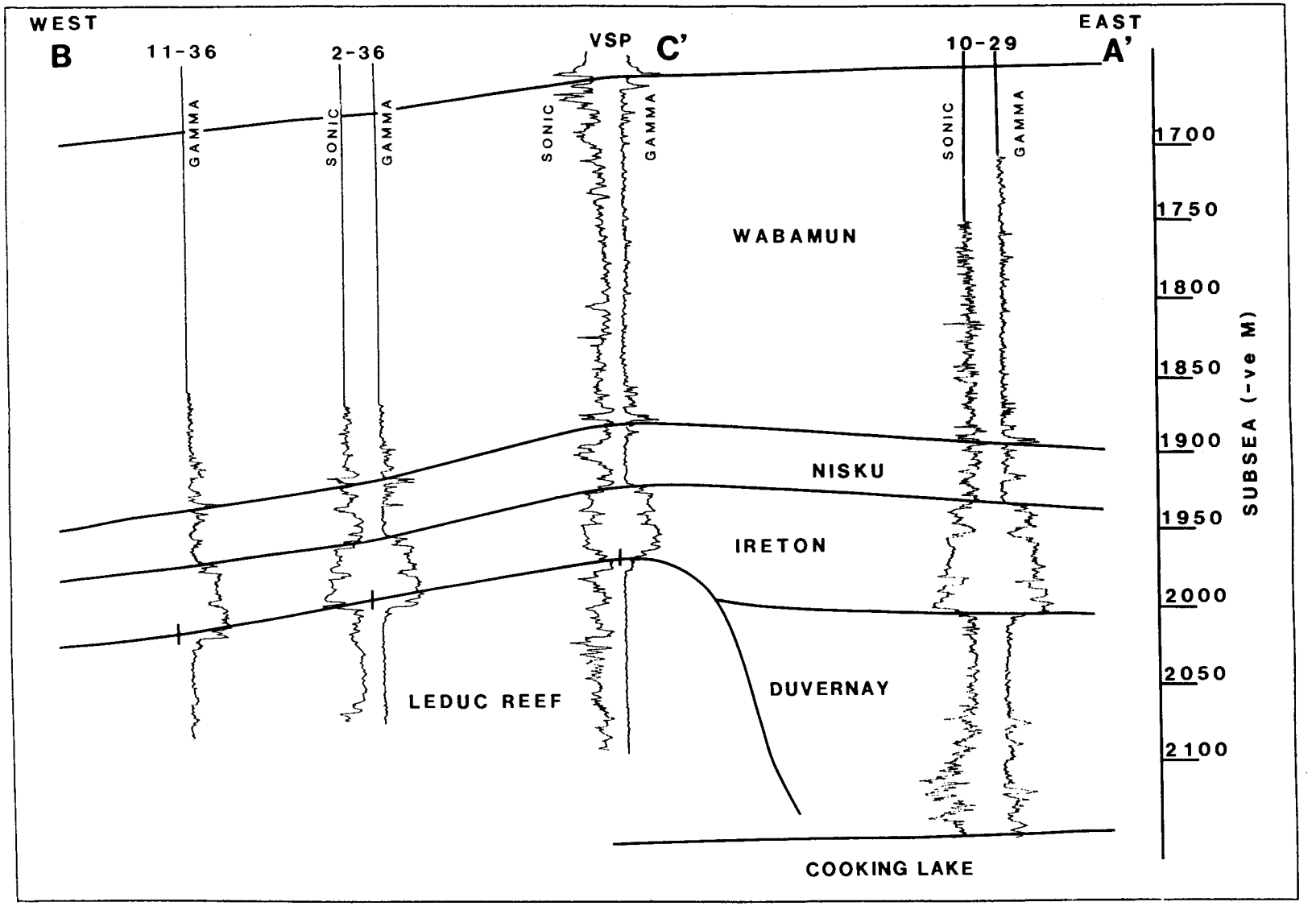

Figure 3.5 West-east geologic cross-section B-A' (refer to Figure 3.3 for location). The Leduc Formation in wells 11-36 and 2-36 (producing oil from the Nisku) is structurally low and wet; the VSP well is productive (Nisku and Leduc Formation oil reservoirs); and well 10-29 is off-reef and abandoned.

restricted to the updip eastern edge (raised rim) of the reef complex (up to 50 m of pay). The eastern and western limits of production are defined by the fore-reef slope and the hydrocarbon/water interface, respectively.

The structural geologic cross-sections (based on the wells located in Fig. 3.3) shown in Figures 3.4, 3.5 and 3.6 illustrate the morphology of the Lanaway complex. Borehole well 10-29 (Fig. 3.4) is off-reef and encountered a full section of inter-reef shale (Ireton and Duvernay); 11-1 is interpreted as having penetrated the structurally low and wet interior lagoon; 16-1 and 11-6 were drilled into the up-dip raised rim of the Lanaway reef and are productive. Well 11-36 (Fig. 3.5) is interpreted as having penetrated the structurally low and wet interior lagoon; 2-36 and the VSP well were drilled into the raised rim of the Lanaway complex. The VSP well is productive. Well 2-36 penetrated the Leduc below the hydrocarbon/water contact; however the well is classified as a Nisku oil well with extended productivity from gas from the Viking Formation of the Cretaceous Colorado Group and oil from the Basal Quartz member of the Ellerslie Formation of the Lower Mannville Group (Lower Cretaceous). These three producing zones (Nisku, Viking and Basal Quartz) are stratigraphically listed in Figures 3.1A-C. The VSP well has a different oil/water contact than 11-6 to the north and, consequently, is assigned to a separate pool. The hydrological barrier between these two wells is related to structural relief at the Leduc level (Fig. 3.6). This relief has been described to be due to several processes or features including surge channels, shale tongues, differential compaction, or original reef morphology by Anderson (1989a, b and c), Klovan (1964) and Mossop (1972).

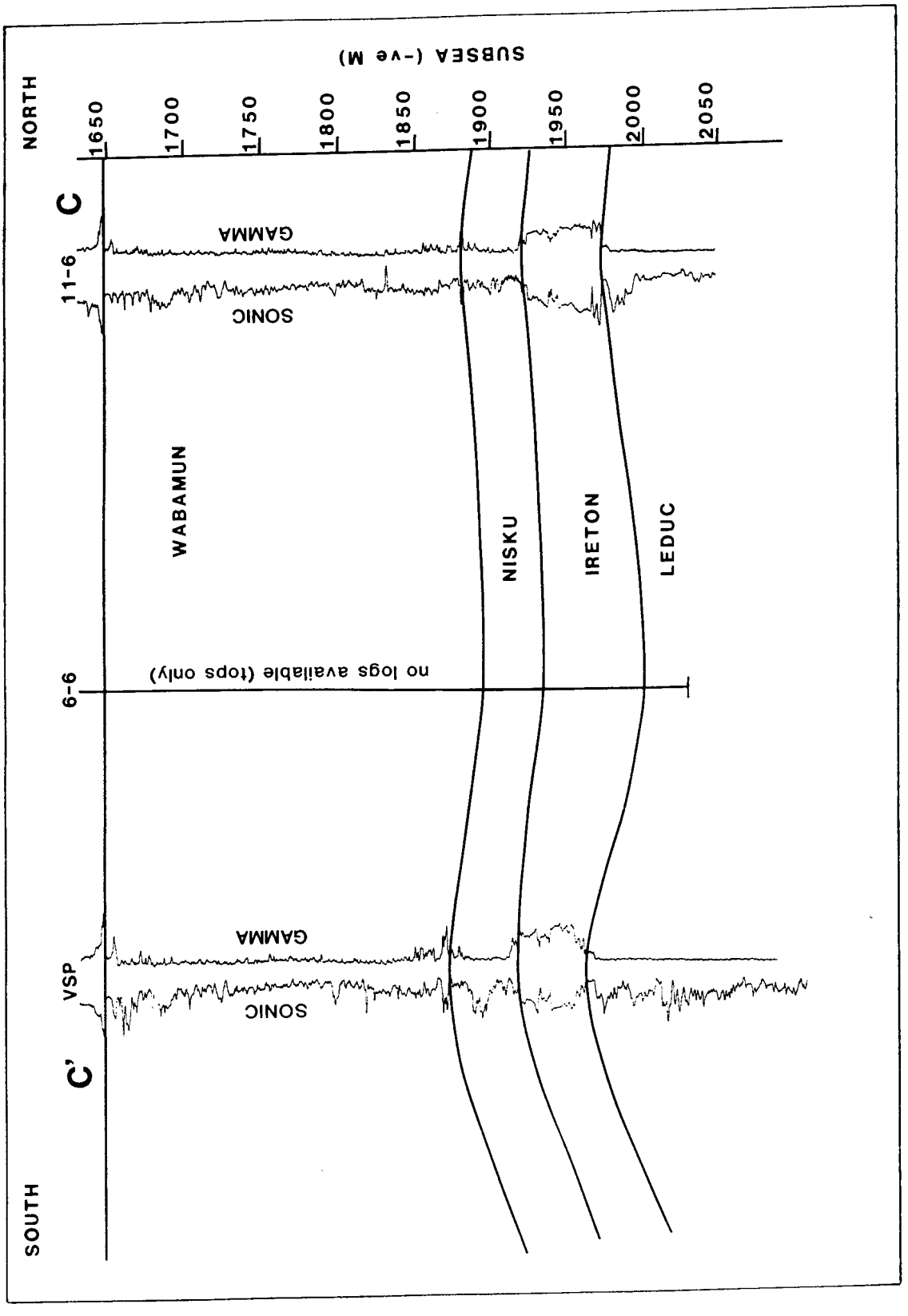

Figure 3.6 North-south geologic cross-section C-C' (refer to Figure 3.3 for location). The Leduc Formation in well 11-6 and the VSP well is productive; and well 6-6 is wet and classified as an abandoned oil well.

The VSP well (Figs. 3.5 and 3.6), although ultimately productive (from both the Nisku and Leduc), was 80 m low at the Leduc level relative to the original seismic prognosis (Hinds et al., 1994a). This pre-drill structural estimate was based on the conventional seismic data interpretation displayed as Figures 3.7 and 3.8. In the original interpretation, the Leduc event is up to 30 ms (80 m) higher between CDP traces 110 and 140 than elsewhere. Geologically, this anomaly was initially envisioned as localized, late stage accretionary reef growth. The drilling of the VSP well however, established that on the original interpretation, the top of the Leduc was miscorrelated by one cycle (between CDP traces 110 and 140). Well log data established that at the VSP well, the Leduc top was more-or-less structurally consistent time-wise with the top of the Leduc elsewhere on the seismic line.

3.4 VSP data acquisition

In an effort to resolve the apparent discrepancy between the surface seismic data (as originally interpreted; Figs. 3.7 and 3.8) and the Leduc top at the VSP well, a VSP survey was designed and conducted at that well site (by myself whilst being employed by Gulf Canada Resources Ltd). The interpretation of the VSP was expected to elucidate:

1) the geological significance (if any) of the misinterpreted seismic anomaly; and

2) the effect of possible multiple interference on the seismic data.

The VSP data were acquired at a single surface offset, located 200 m to the west of the VSP

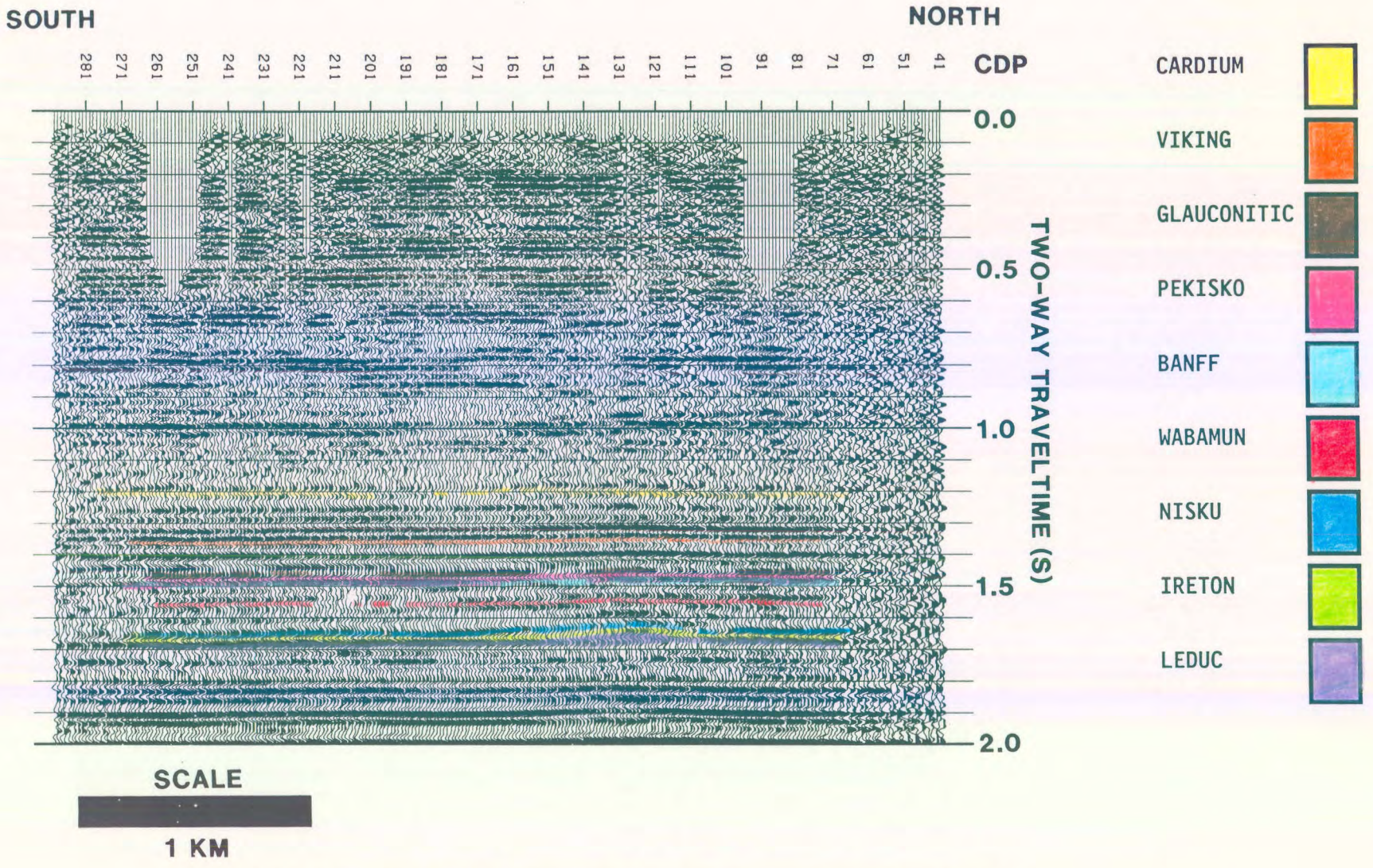

Figure 3.7 North-south oriented example seismic line showing the geophysical interpretation at the VSP well site prior to drilling (refer to Fig. 3.3 for location).

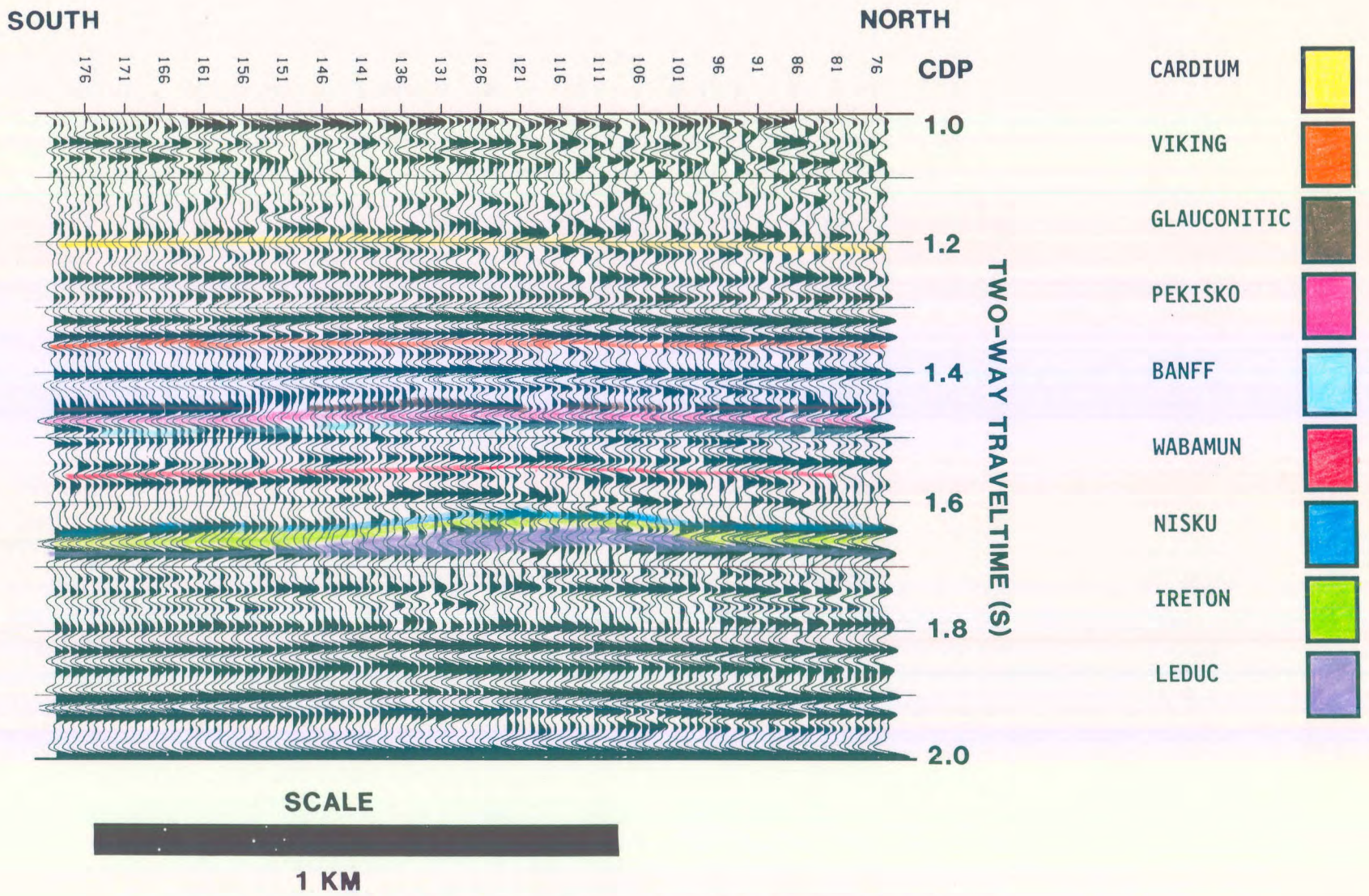

Figure 3.8 Enlarged version of the apparent time-structural anomaly at the Leduc level (shown in Fig. 3.7). The location of the VSP well site is at CDP number 116. (from Hinds et al., 1989a; Hinds et al., 1994a and c).

well on the lease access road. The source consisted of two in-series Vibroseis units utilizing an 8 to 96 Hz input sweep (designed to be compatible with the frequency content of the existing surface seismic data). The Vibroseis sweep was 13 seconds in duration and the recording length was 16 seconds, resulting in a 3 s-long cross-correlated output time series. On average, six sweeps were summed for each subsurface geophone sonde location. The source site was partially frozen and suitable coupling was achieved. The Vibroseis pad location at the offset was shifted periodically by a minor amount to ensure ground coupling stability and to minimize damage to the surface of the lease access road.

The total depth (TD) of the VSP well was 2990 m below the Kelly Bushing (KB) at the time of the running of the VSP survey. The well was drilled slightly further following the survey for stratigraphic evaluation. The elevation of the KB was at 968 m above sea level (asl) and the source at 963 m asl. The geophone sonde was lowered to TD, then raised at 20 m intervals to 2590 m below KB (30 m above the Wabamun Group). Between 2590 and 1315 m (shallowest processed sonde depth location), the sonde recording interval was increased to 25 m. Data were only recorded at three levels above 1315 m (viz at 600, 1000 and 1150 m). These data were acquired principally for sonigram calibration purposes albeit every VSP level first break time and corresponding depth could be used during the sonic log calibration (Hinds et al., 1994c). At each sonde location, the three-component geophone tool was locked in place in the borehole with the locking arm.

The data were recorded at a 2 ms sample interval using the SSC 1078 micro-Vax based system. The recording filter was set at OUT/OUT.

The offset location was chosen to be situated behind a bend in the road so that the source was not in direct line of sight of the well borehole along the lease road (the road was built by the well operator to gain access to the well lease). Another criterion in the choice of the source location was the utilization of a patch of trees that was in the corner of the road between the source and the well which would assist in the reduction of the amplitude of the pseudo-Rayleigh wave propagation along the ground surface thereby aiding in the elimination of groundroll induced interference (tube waves) with the downgoing and upgoing signal.

3.5 VSP interpretive processing

As an aid to the interpretation of the VSP data a suite of interpretive processing panels (IPP's) were generated for these data (Hinds et al., 1989a, Hinds et al., 1991a, 1991b and 1993c, Hinds, 1991c, Hinds et al., 1993a, Hinds et al., 1993b, 1994a and 1994c). The panels allowed the progressive interpretation of the data in order to facilitate the quality control of the processing sequence. More specifically the panels displayed:

1) up- and downgoing P-wavefield separation

2) deconvolution of the separated upgoing P-waves using an inverse filter calculated from the separated downgoing P-waves; and

3) inside and outside corridor stacks of both the deconvolved and nondeconvolved upgoing P-waves.

3.5.1 P-wave separation to output Z_{up}(+TT) data

In the initial phase of processing, the upgoing and downgoing P-waves of the vertical geophone data, **Z(FRT)**, were separated. This separation procedure is illustrated in the wavefield separation IPP (Hinds et al., 1989a and Hinds et al., 1994c) in Figure 3.9.

The **Z(FRT)** data after trace normalization and the gained **Z(FRT)** data are displayed in panels 1 and 2 of Figure 3.9. Several primary upgoing reflections can be identified on these data: viz Viking (at a depth of 2100 m); Mannville (the Glauconitic at 2158 m); and Banff (2293 m). Note that the series of strong reflections that originate below the VSP well TD do not intersect the first break curve, and therefore cannot be confidently classified as either primary or multiple events (Hinds et al., 1989a and Hinds et al., 1994c).

The gained **Z(-TT)** data in panel 3 illustrate that the downgoing wavetrain (the multiples) is comprised mostly of high amplitude surface-generated and less prominent interbed multiples. Surface-generated multiples are recorded on all of the traces and are manifested as laterally continuous events that arrive after the first break events. Interbed multiples, in contrast, do not extend over the entire depth range. If present, they would be present on the deeper traces only (Hinds et al., 1989a).

The downgoing waves contained in panel 3 were separated from the combined wavefield data using an eleven-point median filter and displayed in panel 4, $\mathbf{Z_{down}(-TT)}$. The residual upgoing wave content in the $\mathbf{Z_{down}(-TT)}$ data of panel 4 is minimal. The upgoing waves,

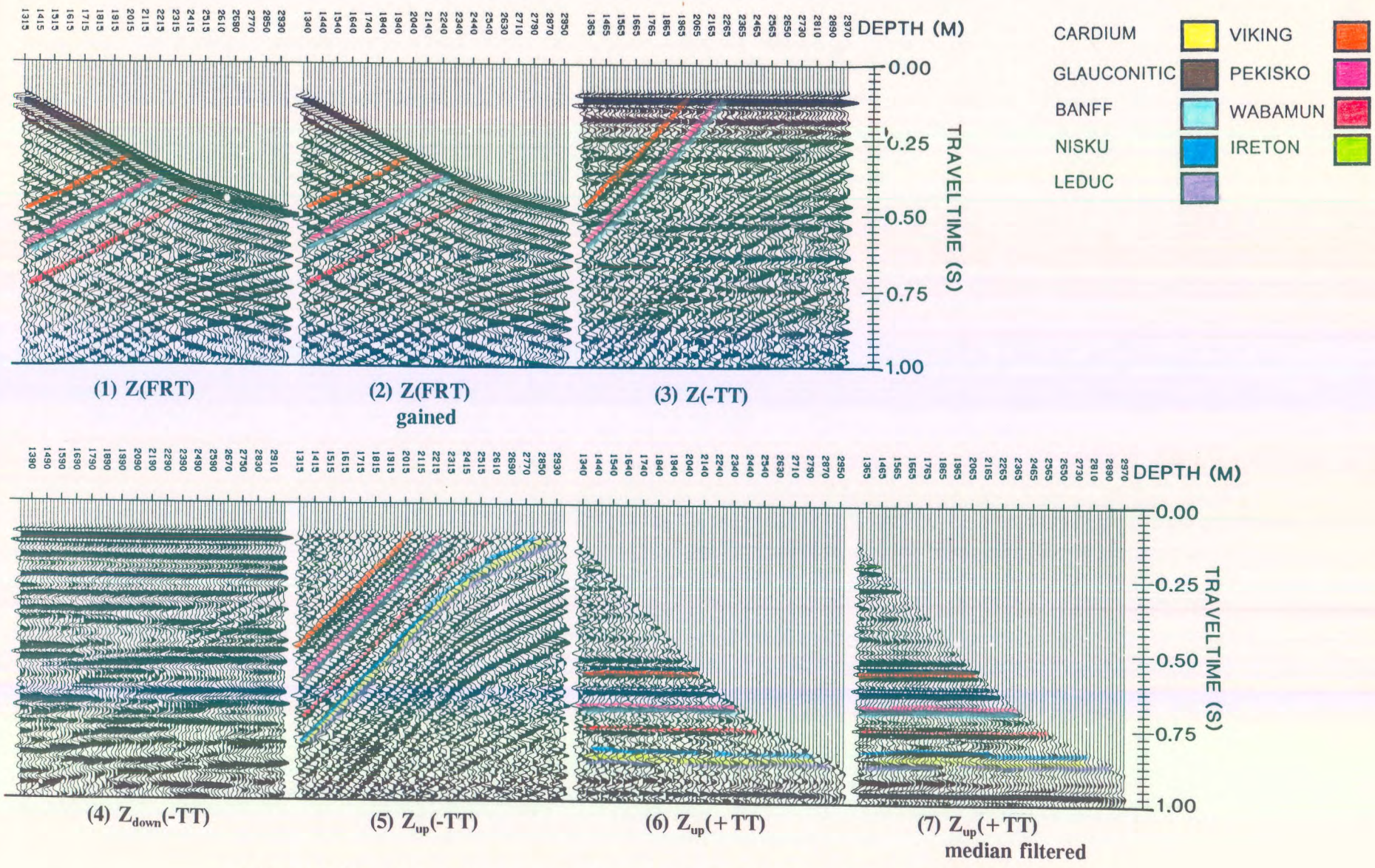

Figure 3.9 Interpretive processing panel depicting the wavefield separation of the near offset VSP data (from Hinds et al., 1989a; Hinds et al., 1994a and c)

$\mathbf{Z_{up}(-TT)}$ in panel 5, were separated by subtracting a scaled version of the downgoing wavefield, $\mathbf{Z_{down}(-TT)}$ of panel 4, from the combined wavefield, **Z(-TT)** of panel 3, following the methodologies described by Balch and Lee (1984), Hardage (1985), Hinds et al., 1989a, Hinds et al., 1994c and others. The two final panels (6 and 7) in the wavefield separation IPP display the separated upgoing waves, $\mathbf{Z_{up}(+TT)}$, before and after the application of a three-point median filter. The equalized amplitudes of the Cardium, Viking, Glauconitic, Pekisko, Banff, Wabamun, Nisku, Ireton and Leduc events in **+TT** time configuration are interpreted in the final panel and confirmed on the previous panels.

Successful wavefield separation is critical to the interpretation of the VSP data, for any residual upgoing wavefield in the $\mathbf{Z_{down}(-TT)}$ data in panel 4, will be subtracted out of the upgoing wave data. Note that the median filter (panels 4 and 5) has not been particularly effective in separating those upgoing waves that arrive after the first break time on the deepest sonde location trace (panel 4). This is acceptable however only because these events are below the zone of interest.

3.5.2 VSP deconvolution

Surface-generated and interbed multiples are totally represented on the separated downgoing wavetrain shown in panel 4 of Figure 3.9. The initial downgoing pulse (except in the case of head wave contamination) is the primary downgoing P-wave; any downgoing waves that arrive later are a result of multiple reflections. These multiple events can be effectively removed by deconvolving the upgoing wave data with an inverse filter derived from an

analysis of the downgoing wavetrain (Hinds et al., 1989a). The deconvolution IPP shown in Figure. 3.10, as reviewed in chapter 2, enables the interpreter to control the quality of the VSP (up/down) deconvolution process (Hinds et al., 1994c). Panels 1, 2, 6 and 7 in Figures 3.9 and 3.10 are bulk time shifted to facilitate the IPP display.

The first two panels (Fig. 3.10) are the unfiltered and median-filtered $\mathbf{Z_{up}(+TT)}$ data. Panels 3 and 4 are the nondeconvolved **Z(-TT)** and $\mathbf{Z_{up}(-TT)}$ data. The fifth panel is the deconvolved upgoing combined wavefield data, $\mathbf{Z_{(decon)}(-TT)}$, and represents an example of downgoing wavefield deconvolution applied to the combined (total) wavefield as first reported in Smidt (1989). The data following the deconvolution step were then wavefield separated, normalized around the first breaks and then corrected for spherical divergence. The deconvolved data were thereafter time shifted to pseudo-two-way traveltime and the resultant $\mathbf{Z_{up(decon)}(+TT)}$ data are displayed in panel 6. A comparison of the median-filter-enhanced nondeconvolved ($\mathbf{Z_{up}(+TT)}$ in panel 2) and deconvolved upgoing ($\mathbf{Z_{up(decon)}(+TT)}$ in panel 7) wavefield data indicates that the deconvolution process has enhanced the frequencies of the upgoing waves and yet preserved the integrity of the primary reflections.

The effect of the interference by multiples and the relative success of the deconvolution operator, can be appreciated by the analysis of the VSP Glauconitic event. In the $\mathbf{Z_{up}(+TT)}$ data in panel 2 (Fig. 3.10), the nondeconvolved Glauconitic event is relatively continuous at sonde depths below the Cardium (1825m). At shallower depths, the Glauconitic event is partially masked by a possible interbed multiple that has as its lower generating surface, the top of the Cardium. On the $\mathbf{Z_{up(decon)}(+TT)}$ data in panel 7, the Glauconitic event is relatively continuous at all the sonde depths implying that the interfering multiple event has

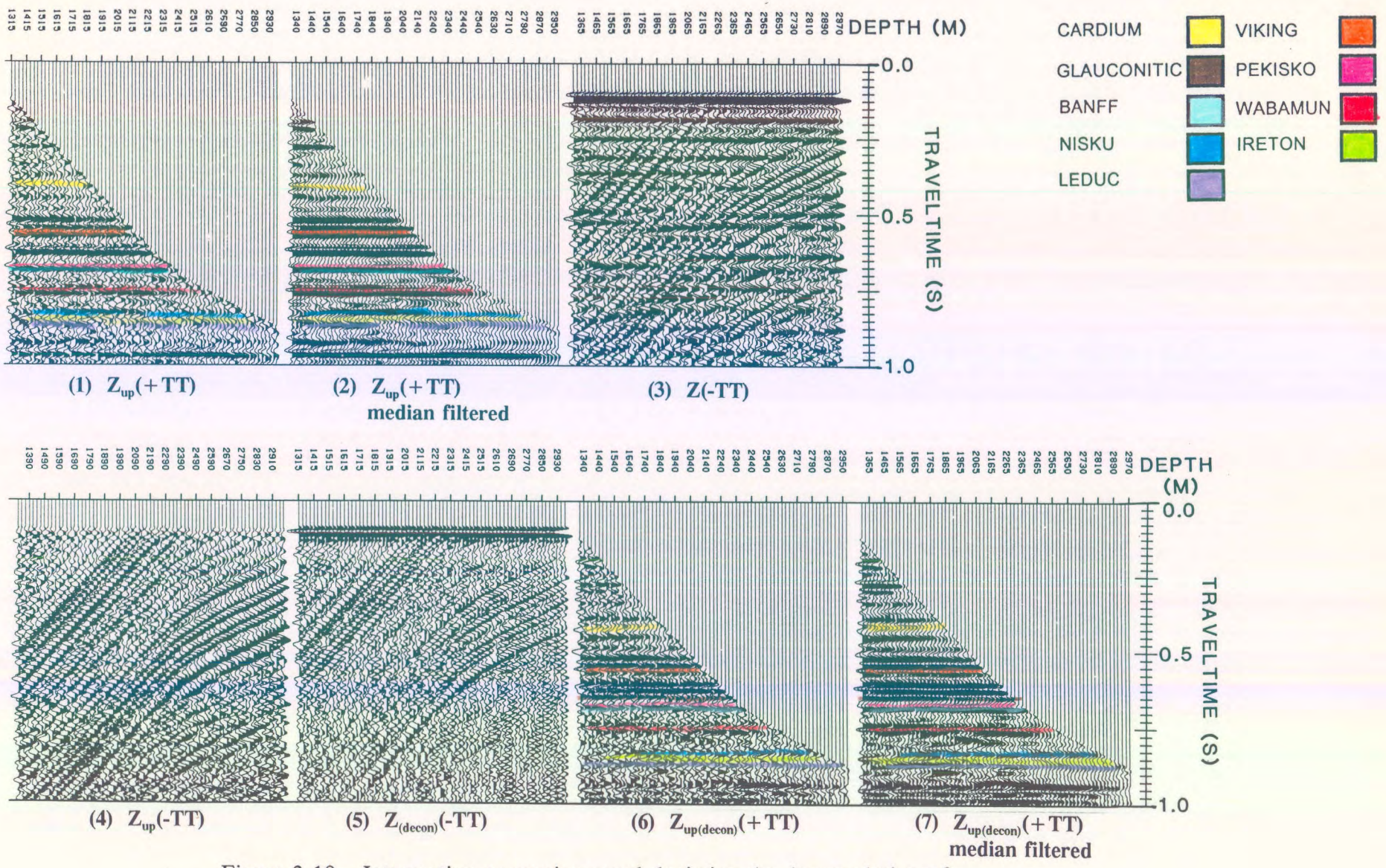

Figure 3.10 Interpretive processing panel depicting the deconvolution of the near offset VSP data (from Hinds et al., 1989a; Hinds et al., 1994a and c).

been attenuated.

Note that the Nisku and Leduc events are relatively low amplitude (in comparison to the Nisku and Leduc events on the seismic line away from the VSP well site) possibly as a result of destructive multiple interference. On the $\mathbf{Z_{up}(+TT)}$ data (panels 1 and 2), a strong peak exists just above (overlapping) the Nisku event from the shallowest trace out to the 2140 m trace. The Nisku event is low amplitude in comparison. After deconvolution, the Nisku event on the $\mathbf{Z_{up(decon)}(+TT)}$ data is laterally continuous in amplitude. The anomalous multiple-induced peak before the deconvolution can be estimated to be up to 5 ms higher than the overlapped Nisku event.

3.5.3 Inside and outside corridor stacks

Multiple contamination on the VSP upgoing waves can be closely examined using the inside and outside corridor stacks of both the $\mathbf{Z_{up}(+TT)}$ and $\mathbf{Z_{up(decon)}(+TT)}$ data. The inside corridor stack of the $\mathbf{Z_{up}(+TT)}$ data contains both the primary and multiple events, whereas the outside corridor stack data should be relatively free of multiples. If the deconvolution is successful in removing the multiples, then both the inside and outside corridor stacks for the $\mathbf{Z_{up(decon)}(+TT)}$ data will be predominated by primary reflections (Hinds et al., 1989a and Hinds et al., 1994c).

In Figure 3.11, the outside and inside corridor stacks are shown in panels 3 and 4, respectively. The input data that are stacked to create the inside and outside corridor stacks are shown in panels 2 and 5. The $\mathbf{Z_{up}(+TT)}$ data shown in panels 1 and 6 are placed beside

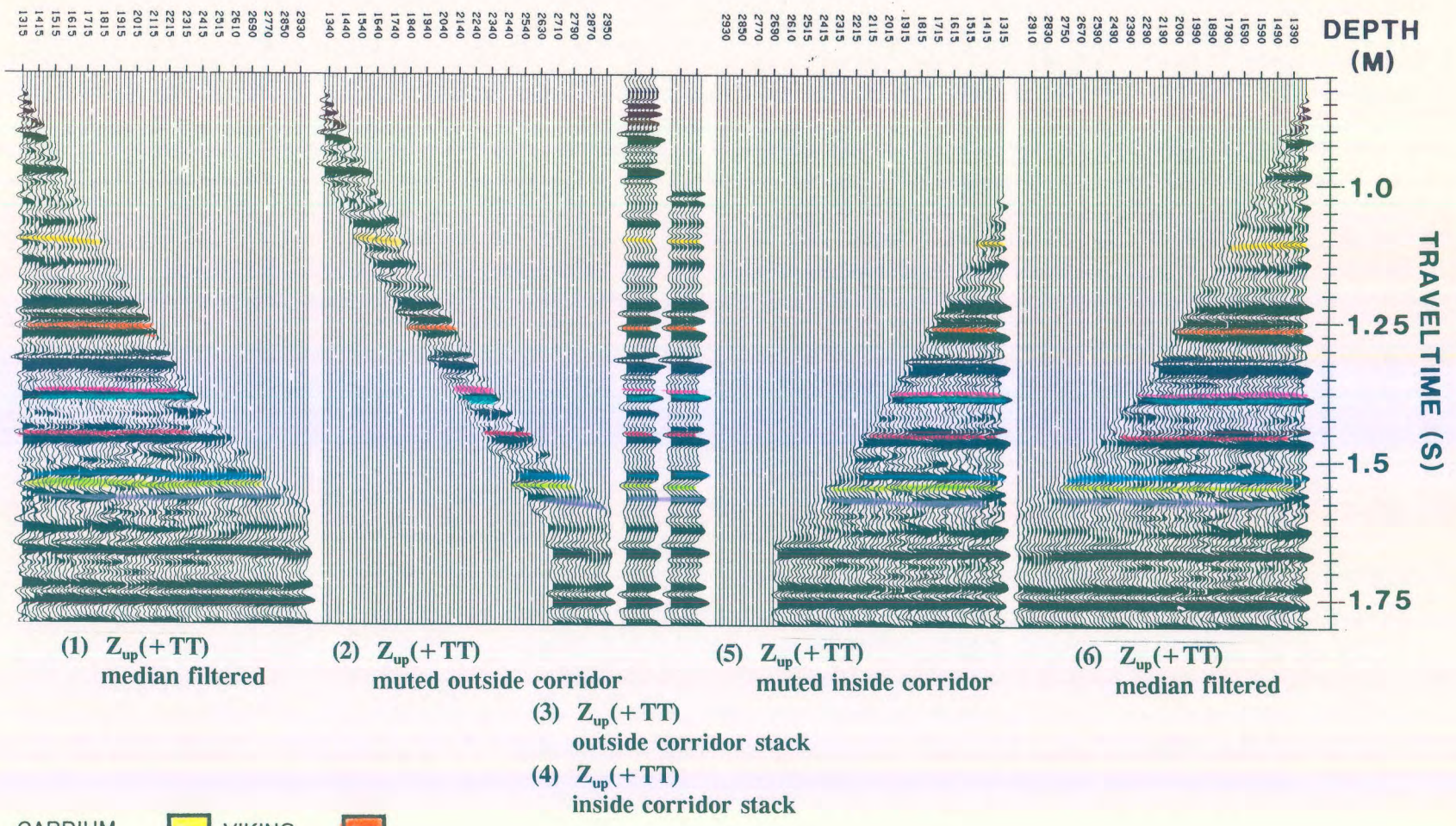

Figure 3.11 Interpretive processing panel illustrating the utility of the nondeconvolved inside and outside corridor stacks for the near offset VSP data (from Hinds et al., 1989a; Hinds et al., 1994a and c).

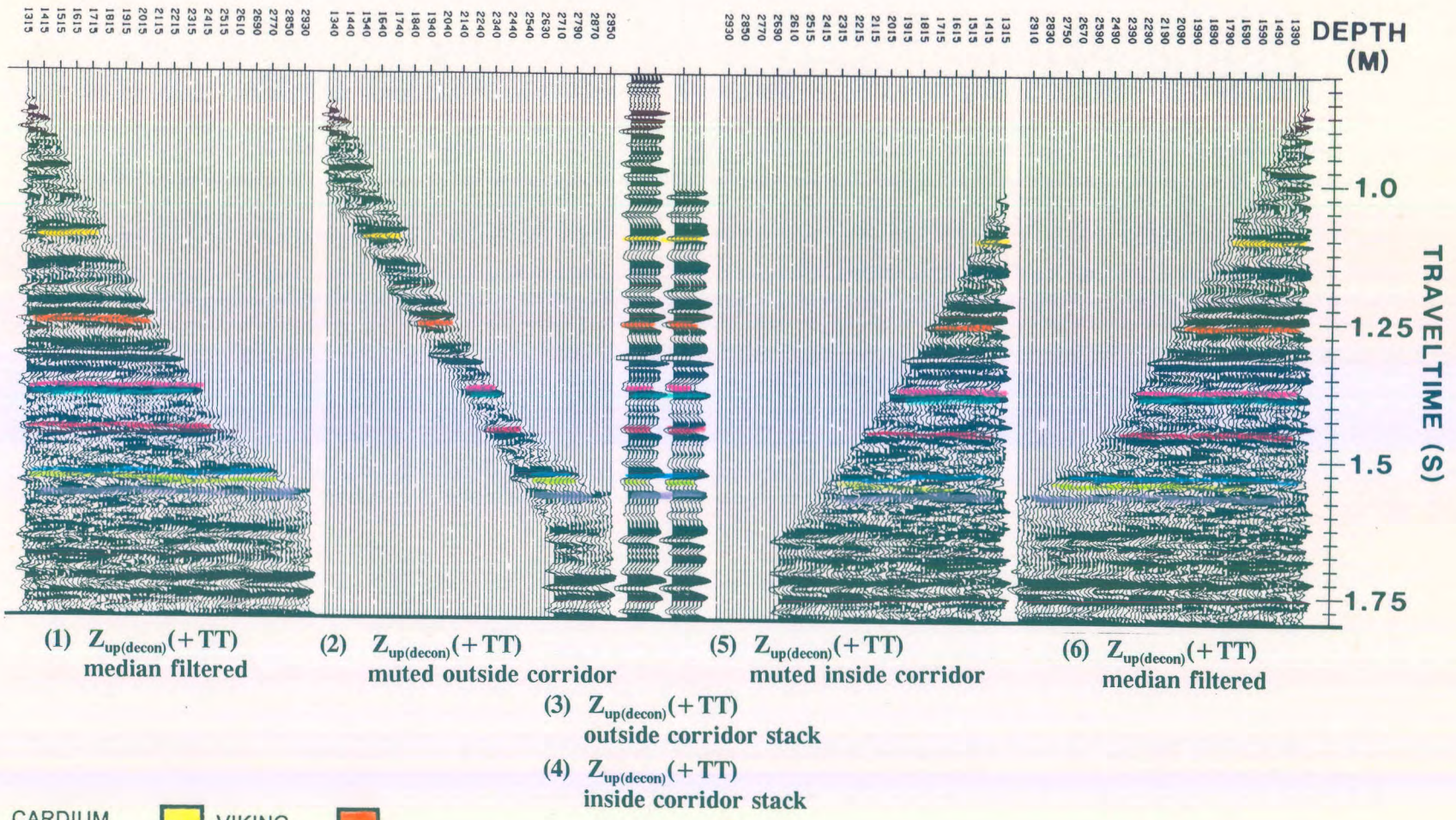

Figure 3.12 Interpretive processing panel illustrating the utility of the deconvolved inside and outside corridor stacks for the near offset VSP data (from Hinds et al., 1989a; Hinds et al., 1994a and c).

the corridor muted $\mathbf{Z_{up}(+TT)}$ data of panels 2 and 5 to show what has been muted.

The inside and outside corridor stacks (panels 4 and 3, respectively) differ below both the Cardium and Banff (at the Wabamun, Nisku and to a lesser degree at the Leduc events) suggesting that multiple interference occurs within these zones. An explanation is that the noticeable effect of the multiples contaminating the inside corridor stack is not represented within the outside corridor stack (Hinds et al., 1994a).

A comparison of the $\mathbf{Z_{up(decon)}(+TT)}$ data inside and outside corridor stacks (Fig. 3.12), indicates that multiple interference was substantially attenuated by deconvolution. More specifically, note that the inside and outside corridor stacks of the $\mathbf{Z_{up(decon)}(+TT)}$ data are similar, suggesting that deconvolution has effectively attenuated the multiple contamination evident on the inside corridor stack of the $\mathbf{Z_{up}(+TT)}$ data (panel 1; Fig. 3.11).

3.6 Integrated interpretation

The reinterpreted conventional surface seismic line incorporating the VSP results (Figs. 3.7, 3.8, 3.14, and 3.15) is displayed on the left-hand side of Figure 3.13. A synthetic seismogram for the VSP well, the $\mathbf{Z_{up}(+TT)}$ data inside corridor stack, and the $\mathbf{Z_{up(decon)}(+TT)}$ data outside corridor stack are time-tied to the seismic line at the VSP well site (CDP number 127). The inside and outside corridor stacks and the synthetic seismogram, juxtaposed between the two separated parts of the seismic section at the VSP well location, allows a comparison between the three methods of the time-tie to the Leduc surface seismic event.

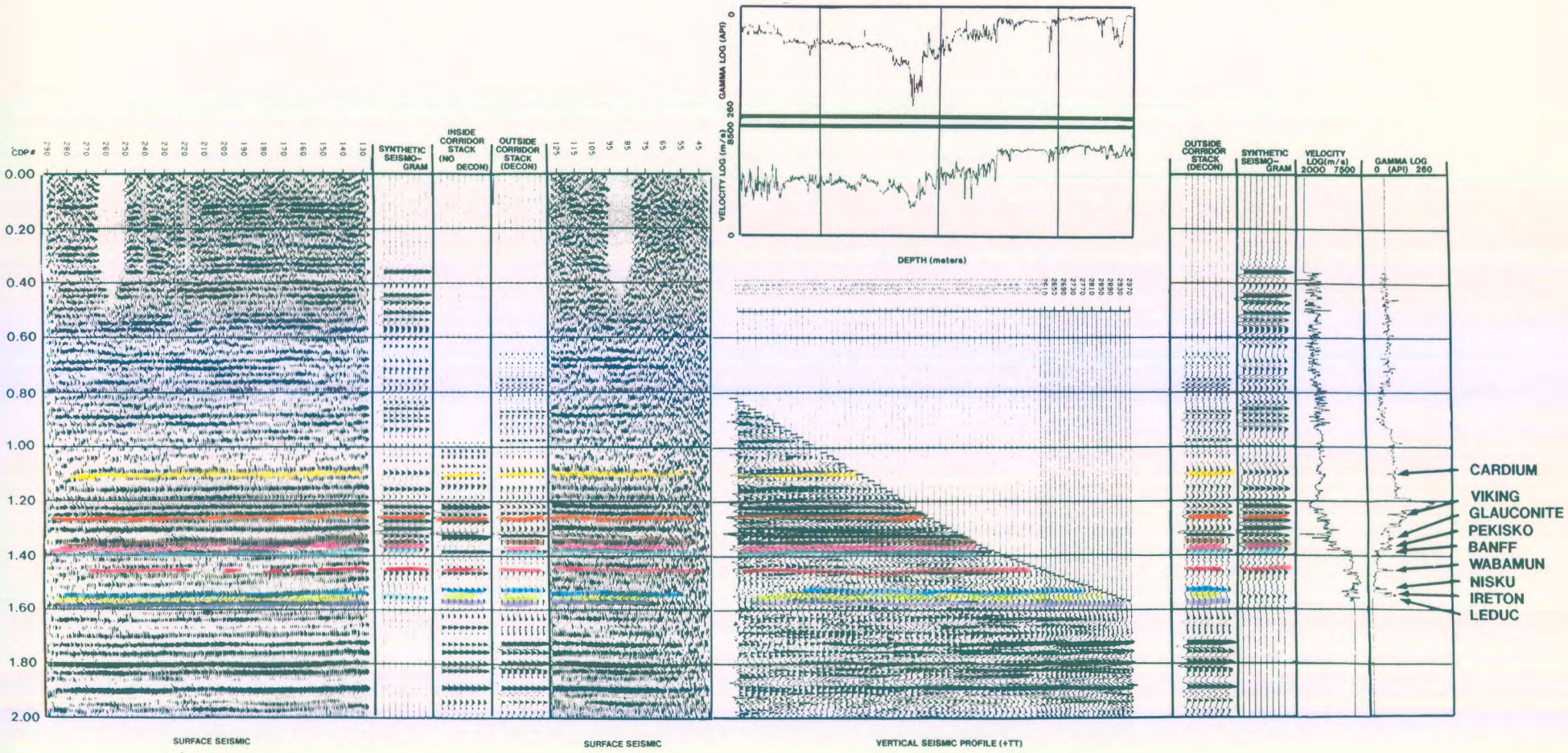

Figure 3.13 Integrated interpretive display (IID) showing the interpretation of the available exploration data for the Lanaway Field case study. The synthetic seismogram was generated using a zero-phase, 30 hz centre frequency Ricker wavelet (from Hinds et al., 1989a; Hinds et al., 1994a and c).

On the right-hand side of Figure 3.13, the VSP data are time-tied to the seismic line, the $\mathbf{Z_{up(decon)}(+TT)}$ data outside corridor stack, the VSP well synthetic seismogram, the VSP well velocity log, and the VSP well gamma ray log. The horizontal scale (depth axis) of the VSP display, $\mathbf{Z_{up(decon)}(+TT)}$, and the scale used for the horizontally-oriented VSP well sonic and gamma ray log depth displays are the same. The outside corridor stack (containing predominantly primary events), the synthetic seismogram, and the two well logs (converted to time) allows for the comparison of the corridor stack, the synthetic seismogram, and the well log data. Because the synthetic seismogram is calculated from the sonic log (where the sonic data are virtually collected continuously) in the same area, the synthetic will have higher resolution than the corridor stack. Since the range of the wavelengths contained in the $\mathbf{Z_{up(decon)}(+TT)}$ data are the same as for surface seismic, in most cases the outside corridor stack interpretation will tie to the seismic data interpretation more closely.

The VSP well sonic and gamma logs are displayed in depth and plotted immediately above the $\mathbf{Z_{up(decon)}(+TT)}$ data in Figure 3.13. The correlation between these data can be illustrated by considering the top of the Wabamun.

Lithologically, the top of the Wabamun in the VSP well is represented by the shale/carbonate contact at a depth of 2616 m. Within the VSP data, there are recorded VSP traces at 2610 m and then below the Wabamun formation top is at 2630 m. The Wabamun event is therefore identified as the trough (some interpreters prefer to use the zero-crossing) located in time between the first breaks for the 2610 and 2630 m sonde depths (approximately 1450 ms). In a similar fashion, the other VSP upgoing events can be identified and then correlated directly to the surface seismic line at CDP number 127, the nondeconvolved inside corridor

stack, the deconvolved outside stack, and the synthetic seismogram, velocity and gamma log (displayed in time) for the VSP well.

The location of the Leduc event is of the greatest interest to the interpreter. Note that this reflection, on the surface seismic and VSP data at the VSP well site, is a half cycle lower than initially interpreted by the owners of the data (pre-VSP interpretation shown in Figs. 3.7 and 3.8). The revised surface seismic interpretation is presented in Figures 3.14 and 3.15. A correlation of the VSP and the surface seismic data indicates that the Leduc top was incorrectly identified at the VSP well site on the pre-VSP interpretation. This miscorrelation explains why the Leduc top came in 80 m low relative to prognosis; however, it does not explain why the surface seismic line was originally misinterpreted. Anomalous Nisku, Ireton and Leduc surface seismic signatures between CDP numbers 90 to 140 may have resulted in a misleading interpretation (Figs. 3.14 and 3.15).

This seismic package from the Wabamun to the Leduc events is characterized by:

1) positive time-structural relief (of the order of 5 ms) along both pre-Leduc and deeper post-Leduc events;

2) an anomalously low-amplitude Leduc event; and

3) an anomalous reflection pattern within the Wabamun/Leduc interval (drape over the reef edge by the Wabamun and the Nisku events).

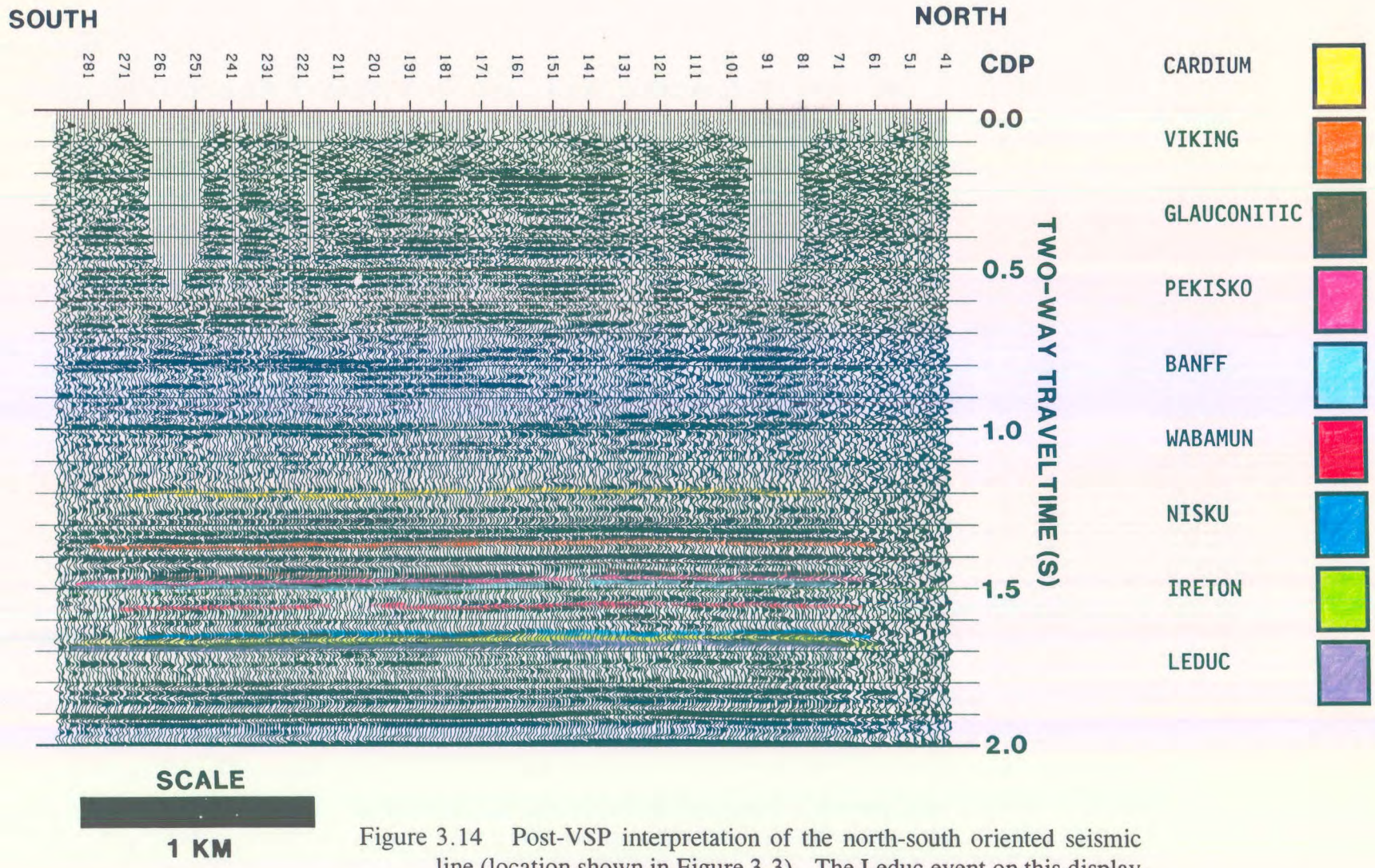

Figure 3.14 Post-VSP interpretation of the north-south oriented seismic line (location shown in Figure 3.3). The Leduc event on this display is only slightly time-structurally elevated at the VSP well site and the updated interpretation is consistent with well log control (from Hinds et al., 1989a; Hinds et al., 1994a and c).

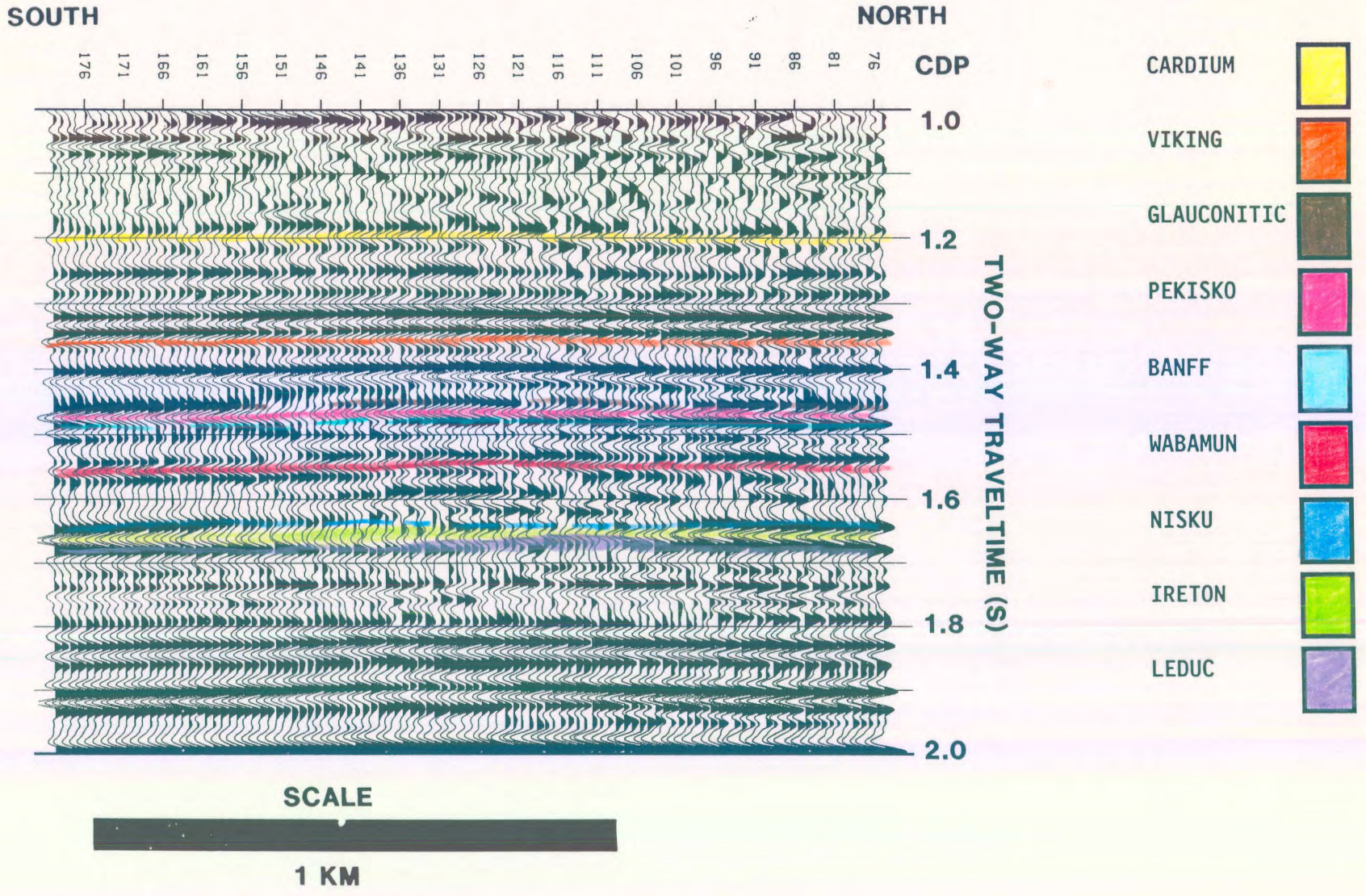

Figure 3.15 Enlarged version of the post-VSP interpretation of the north-south oriented seismic line (shown in Fig. 3.14). The VSP well location is at CDP number 116 (from Hinds et al., 1989a; Hinds et al., 1994a and c).

These three types of seismic signatures were initially interpreted to be diagnostic of the reef and were attributed to an envisioned 80 m of anomalous accretionary reef growth. The time-structural relief in particular was attributed to velocity pull-up and drape, respectively.

The VSP well dataset conclusively established that the Leduc was misidentified on the original interpretation (Figs. 3.7 and 3.8) and that the observed seismic anomalies are not related to late stage accretionary reef growth (Hinds et al., 1994a). There appear to be three most probable candidates for the explanation for the seismic anomaly:

1) structural relief at the Pekisko and Shunda pre-Cretaceous subcrops;

2) stratigraphic anomalies (possible patch carbonate reef) within the Winterburn Group (Fig. 3.1c); and

3) structural thinning of the Ireton near the reef crest (as shown in Fig. 3.6).

Dealing with the first explanation, it is conceivable that the observed anomaly is partially caused by erosional relief at the pre-Cretaceous subcrop (Pekisko and Shunda). As illustrated by the velocity log (Fig. 3.13), the velocity of seismic wave propagation of the Shunda and Pekisko Formations are higher than those of the overlying Cretaceous sediment. Positive erosional relief at the Shunda/Pekisko level would cause pre-Cretaceous events to be time structurally "pulled-up", and the overlying seismic events would appear to be anomalously draped as a result of compaction of the formations above the Pekisko and Shunda material (Anderson et al., 1989a). However, no Shunda Formation material was intersected at the

VSP well in comparison to 14 m at the 6-6 well location (as shown in the Shunda isopach map in Fig. 3.16). The combined Shunda/Pekisko thicknesses at the VSP well and 6-6 are 43 and 55 m, respectively.

The second suggested explanation for the observed time-structure and amplitude anomalies is a lithologic variation within the Winterburn Group. It is possible that a localized Nisku Formation (Winterburn Group) patch reef has developed above the crest of the underlying Leduc reef (similar to the patch reef suggested in the case study in Rennie et al., 1989). The envisioned carbonate build-up would be characterized by a velocity pull-up, time-structural drape, and a character change within the Winterburn Group. Unfortunately, due to the absence of core control within the Winterburn Group, this suggestion cannot be confirmed or negated; however it should be noted that the VSP well and well 6-6 intersected 47.4 and 39.3 m of Nisku, respectively. The added Nisku build-up and corresponding porosity could conceivably contribute to the observed time-structural anomaly. The patch reef could have resulted from the localized structural high resulting from the presence of the reef edge.

The third possibility suggested is that subtle draping of Ireton sediments above the reef crest at the VSP well as has already been highlighted in the north-south geologic cross-section shown in Figure 3.6 could be the cause of the misinterpretation. The isopach map of the Ireton in Figure 3.17 shows that the north-south oriented seismic line (Figs. 3.7 and 3.8) traverses a thick succession of Ireton shales at well 6-6 (66 m), while it is relatively thinner over the reef crest at the VSP well (43 m) and it thickens in LSD 30 towards well 6-30.

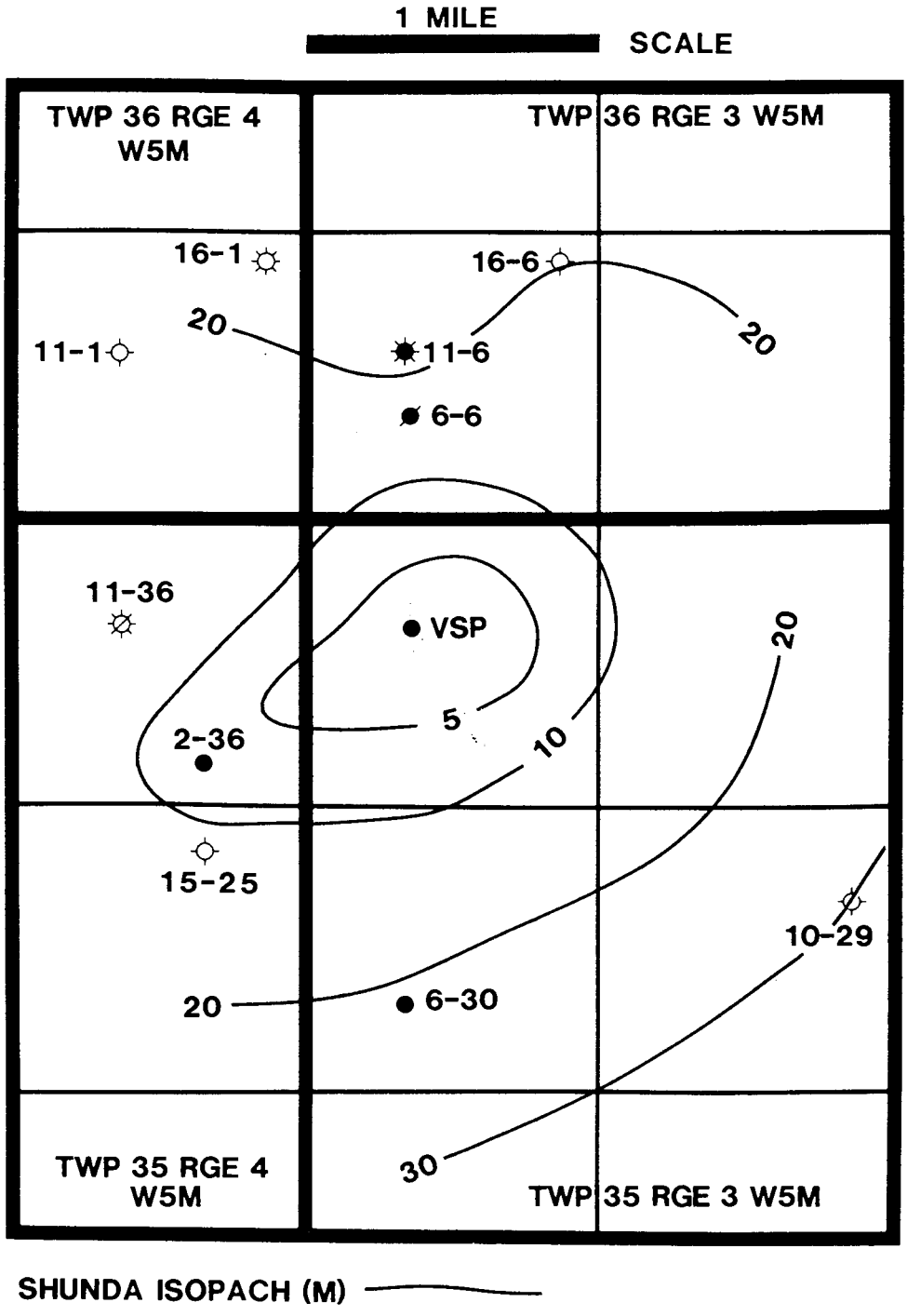

Figure 3.16 Shunda isopach map showing the absence of Shunda at the VSP well. The pre-Cretaceous anomaly may reflect only to a minor to negligible degree a possible source of the seismic defocussing seen on the seismic image of the Ireton to Leduc events at the VSP well (from Hinds et al., 1994a and c).

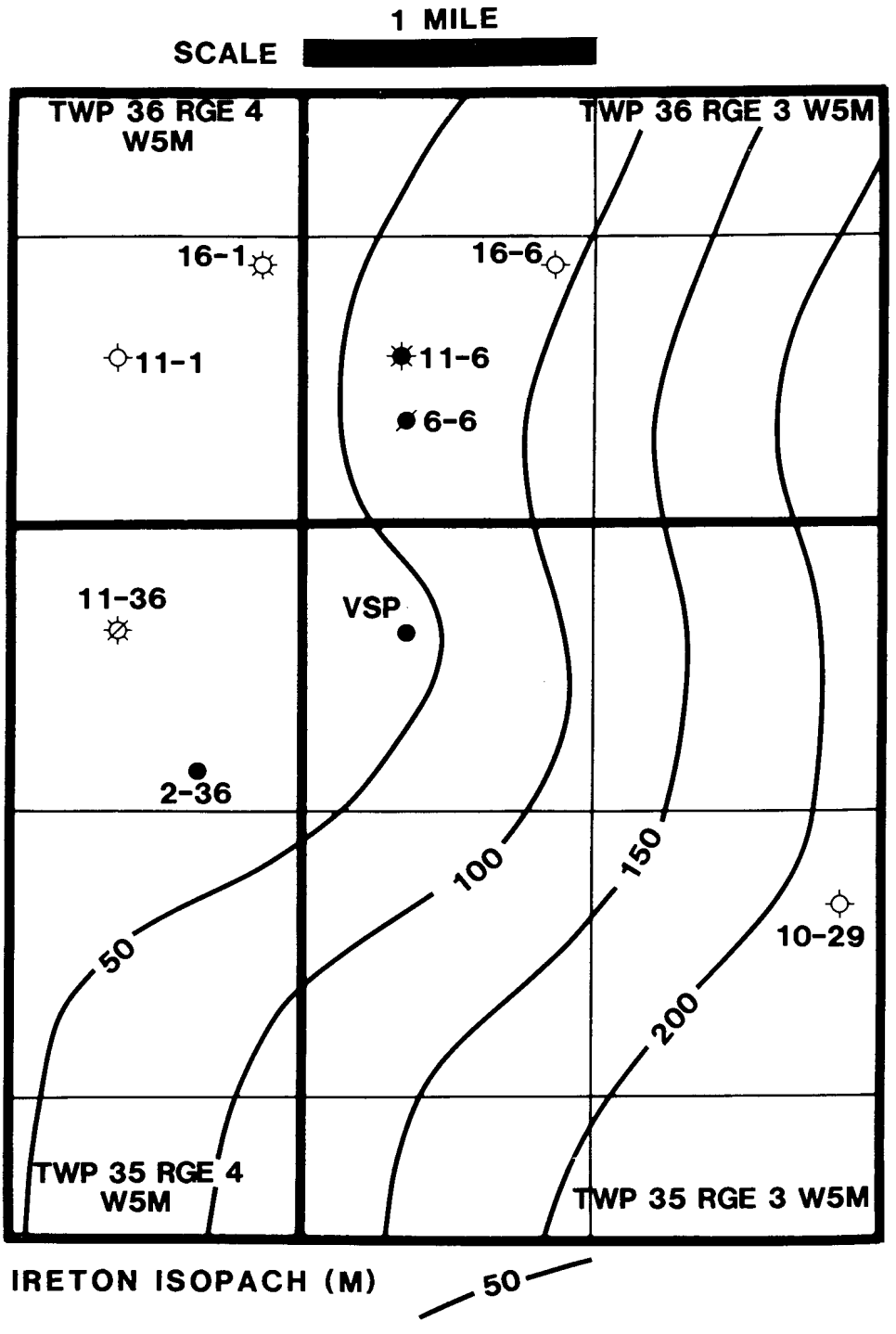

Figure 3.17 Ireton isopach map showing the drape of the Ireton shales along the example seismic line (shown in Figs. 3.14 and 3.15). Considerable time-structural relief along the Ireton event can be correlated from the seismic to the isopach map (from Hinds et al., 1994a and c).

LSD 30 is the mile by a mile section of land directly south of the LSD in which the VSP well was drilled and is shown in Figure 3.17. The Nisku to Ireton anomalous isochron values that are evident at the VSP well location return to normal ranges approximately 640 m south of the VSP well along the seismic line (Fig. 3.17). This can be seen at CDP number 200 in Figure 3.7 and corresponds to the location of the intersection of the seismic line and the 100 m Ireton isopach contour in Figure 3.17. The correlation of the seismic anomaly at the Nisku, Ireton and Leduc levels to the Ireton isopach suggests that the increasing Ireton isopach (away from the well both to the North and South) caused an anomalous seismic response to the subtle drape over the reef crest at the VSP well and this tuning effect can be contributing to the seismic event anomaly (drape and pullup) at the VSP well.

The initial interpretation of the seismic events at the VSP well could then be resolved to be caused by a combination of thinning of the Ireton Formation and an increasing porosity thickness of the Nisku Formation. Part of the Nisku Formation material could be productive as indicated by an anomalous velocity character in the sonic logs (possible patch reef carbonates) that begins approximately 10 m below the Nisku top in the VSP well.

Furthermore, from the inside and outside corridor stacks of both the $\mathbf{Z_{up(decon)}(+TT)}$ and the $\mathbf{Z_{up}(+TT)}$ data as displayed in Figures 3.11 and 3.12, it is apparent that there is multiple contamination immediately below the Wabamun event that may cause difficulties with the interpretation of the Wabamun throughout the study area, and at the Nisku level. However, the effect of the multiple at the Nisku level can account for no more than 5 ms of the anomaly and therefore would be a minor factor in possible causes of the seismic anomaly

around the VSP-well.

Other interesting observations can be made from the integrated sonic log, VSP corridor stacks and the seismic data in the immediate vicinity of the VSP well. The Glauconitic to Banff sequence and top of the Leduc are poorly resolved on the surface seismic data (relative to the outside corridor stack). One possible explanation is that the surface seismic signatures of events within the Glauconitic to Banff interval may be degraded as a result of multiple (interbed) interference.

The correlation of the data presented in Figure 3.13 has allowed for the confident reinterpretation of the surface seismic data in the vicinity of the VSP well, and further elucidated the possible origin of the observed anomaly. These reinterpreted seismic data are displayed as Figures 3.14 and 3.15. (The anomaly in the immediate vicinity of the VSP well is enlarged in scale and displayed in Fig. 3.15.)

3.7 Discussion on integrated interpretation

The VSP well was drilled into the Leduc reef at Lanaway Field, south-central Alberta, in order to evaluate an anomaly observed on surface seismic data. The pre-well interpretation of these seismic data suggested that the VSP well would encounter up to 80 m of anomalous accretionary reef growth at the Leduc level. However, drilling confirmed that the Leduc at the VSP well was more-or-less regional and indicated that the initial interpretation was inaccurate as the seismic events were a response to something other than anomalous Leduc buildups and corresponding anomalous Ireton thinning. In order to elucidate the discrepancy between the pre-well seismic interpretation and the drilling results, a near-offset VSP was run at the VSP well site.

The interpretively processed VSP data provided invaluable information regarding the seismic anomaly. On the basis of these data, it was possible to:

1) establish that the Leduc event had been miscorrelated on the pre-well seismic interpretation;

2) correctly correlate the Leduc event at the VSP well site; and

3) further elucidate the nature of the observed anomaly at the VSP well site.

On the basis of VSP data and the integrated interpretation, it has been suggested that the

observed seismic anomaly at the VSP well is most likely attributable to (Hinds et al., 1994a):

1) velocity and structural drape resulting from anomalous erosional relief at the pre-Cretaceous subcrop, and the effects of associated interbed multiple reflections;

2) localized patch reef development within the Winterburn Group; and

3) tuning resulting from thinning of the Ireton Formation in the vicinity of the VSP-well.

The most likely effects are the Winterburn patch reef and the tuning effect of an Ireton drape.

CHAPTER 4

THE RICINUS FIELD CASE STUDY

On the basis of the interpretation of conventional surface seismic data, an exploratory well (locally referred to as the VSP well in this chapter) was drilled in the Ricinus Field, southern Alberta, Canada. The prognosis was that the VSP well would encounter the updip, raised rim of the Leduc Formation (Devonian Woodbend Group) reef complex at Ricinus Field, and would penetrate on the order of 140 m of gas pay. To the consternation of the exploration team, the well encountered only off-reef shales. The Ricinus Field had been previously defined by existing wells; some of which are shown in Figure 4.1.

As part of an investigation into the seismic images of the surrounding area, two vertical seismic profiles were conducted at the VSP well site in an effort to:

1) resolve the apparent discrepancy between the interpreted surface seismic data and the geology at the VSP well; and
2) evaluate the feasibility of whipstocking the VSP well in the direction of the reef complex.

One of the VSP surveys had a source offset of 199 m (near offset) and the other had a source offset of 1100 m (far offset). These data allowed the more confident and geologically consistent reinterpretation of the surface seismic data, and clearly indicated that whipstocking was not an economically viable option (Hinds et al., 1989a; Hinds et al., 1993c; and Hinds

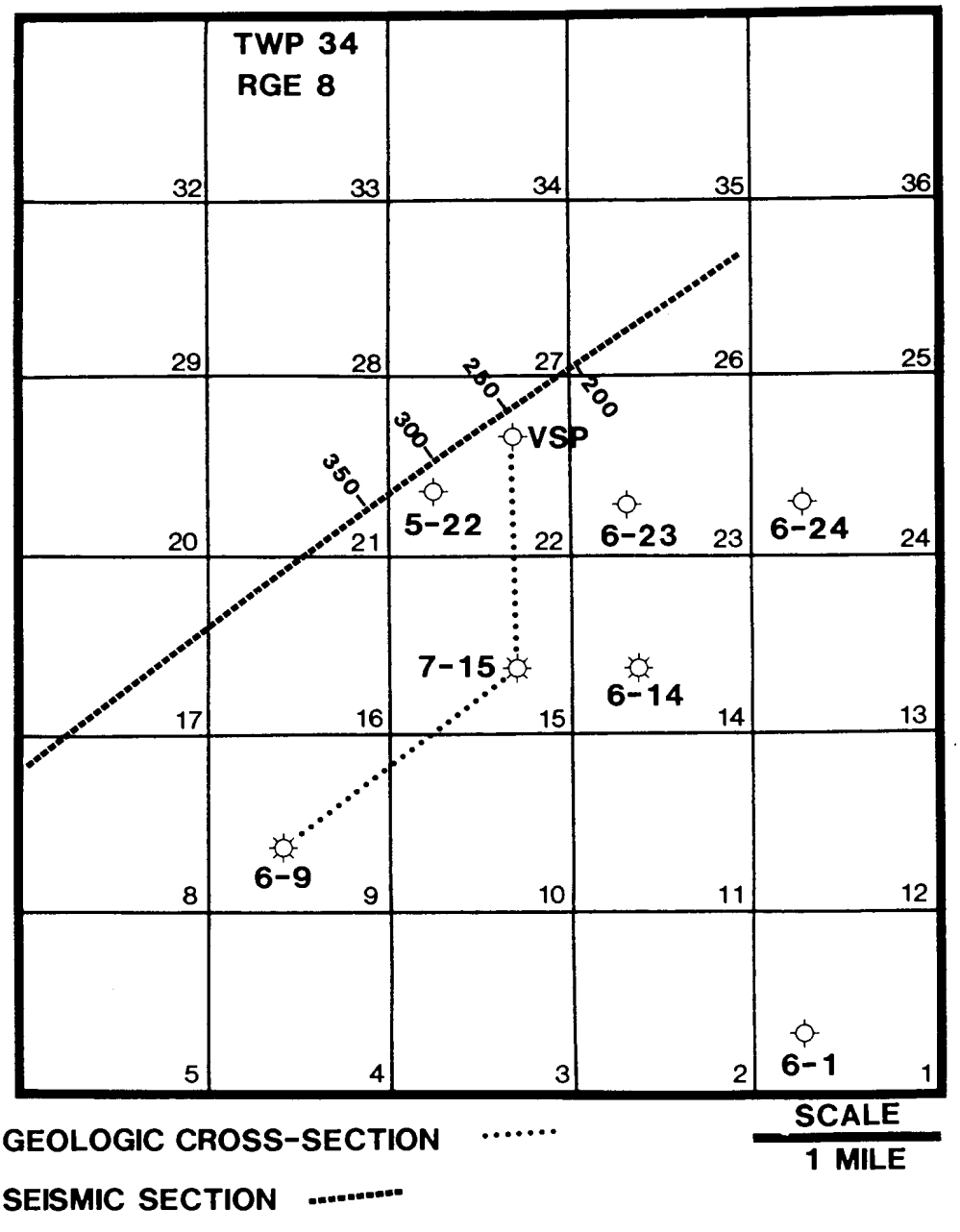

Figure 4.1 Detailed map of Ricinus study area showing the location of the wells used in the geological schematic section shown in Figures 4.2 and 4.4, the seismic data shown in Figures 4.3, 4.5 and 4.17, and locations for Leduc Formation level wells in the Ricinus Field area (from Hinds et al., 1993c; Hinds et al., 1994c).

et al., 1993c). Towards these ends, the VSP was relatively successful.

In this chapter, I present a case history that illustrates the potential for the misinterpretation of 2-D surface seismic data in the Ricinus area. This study is based on a situation where the plausible, yet ultimately inaccurate interpretation of surface seismic data led to the drilling of the VSP well. The VSP well was expected to intersect the updip edge of the Ricinus Leduc reef according to the original interpretation shown in Figure 4.2. Unfortunately it encountered only off-reef shales and was abandoned. Herein, I discuss the VSP well results, and the surface seismic and VSP data signatures at the VSP well site. The 2-D data presented were acquired prior to drilling the exploratory VSP well. The VSP survey was run in an attempt to resolve the discrepancy between the initial (pre-VSP well) interpretation of the surface seismic data and the geology at the VSP well site and to seismically image laterally away from the well towards the Southwest.

4.1 The Ricinus Field

The stratigraphy of the Ricinus Field is similar to that of the Lanaway field (Figs. 3.1A, B, and C). Similar to the situation at the Lanaway Field, the Leduc Formation at the Ricinus Field (Figs. 3.2 and 4.1), is interpreted as a large atoll which towers some 350 - 400 m (based on well 6-9-34-8 W5M) above the Cooking Lake platform and appears to exhibit a mappable peripheral raised rim and a structurally lower central lagoonal area. As at the Lanaway Field, the updip edge (northeast) of the raised rim at Ricinus is productive where it is structurally closed and effectively sealed by the inter-reef shales of the Duvernay and

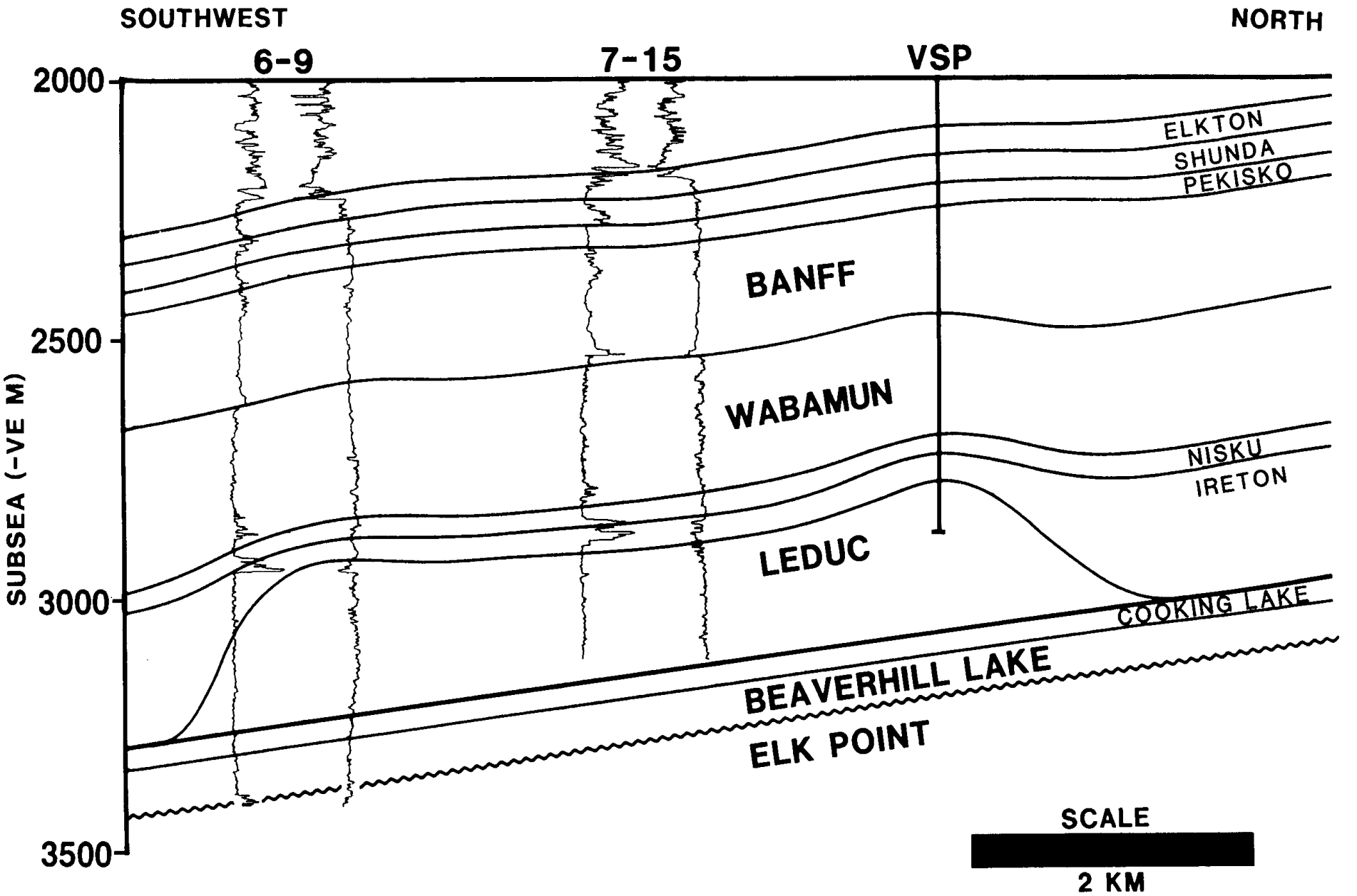

Figure 4.2 Schematic section depicting the envisioned subsurface geology at the VSP well site prior to the drilling of the VSP well. This interpretation is based on downhole data from wells 6-9-34-8 W5M and 7-15-34-8 wells and the seismic interpretation shown in Figure 4.3. The geology data from the VSP well confirmed that the seismic interpretation is incorrect. The preferred, current interpretation is shown in Figure 4.4 (from Hinds et al., 1993c; Hinds et al., 1994c).

Ireton. The schematic cross-section shown in Figure 4.2 illustrates the interpreted morphological relationships between the Leduc and the inter-reef shales of the Ireton and Duvernay in the Ricinus area (Hinds et al., 1989a, Hinds et al., 1993c; Hinds et al., 1994c).

In those areas of western Canada where the Devonian and/or overlying rock units are relatively undisturbed structurally, full Leduc reefs and inter-reef shales can usually be differentiated on seismic data. These carbonate build-ups are typically characterized by appreciable velocity pull-up (up to 25 ms), significant time-structural drape at the top of the Devonian (up to 70 ms at Ricinus in contrast to 25 ms at Lanaway), and character variations within the Woodbend Group (Anderson and Brown, 1987). Back from their steeply dipping margins, the tops of these reefs are generally manifested as high-amplitude troughs on reverse polarity seismic data (Hinds et al., 1993c).

The examples of low-relief reefs described by Anderson et al., (1989a), Anderson et al., (1989b) and Hinds et al., (1993b) are characterized by less than 10 ms of velocity pull-up and less than 20 ms of time-structural drape. Additionally, the reflections from the top of the reefs are difficult to differentiate from the inter-shale events. In those areas where extensive subsurface structural deformation has occurred, even the seismic image of the full Leduc reef may be effectively masked by the superimposed seismic signature of the structural complexities. Thrust faulting within Mesozoic strata in the general area of the Ricinus reef for example, can significantly affect the seismic signature of the Leduc reefs (Hinds et al., 1993c).

4.2 Ricinus Leduc reef

The diagrammatic cross-section incorporating wells 6-9, 7-15 and the VSP-well, shown in Figure 4.2, summarizes the geological and geophysical interpretation at the VSP well site prior to the drilling of the VSP well. This cross-section was based on the initial (pre-VSP well) interpretation of the example seismic data (Fig. 4.3), and well control available at that time.

The location and corresponding CDP numbers for one of the seismic sections used in the initial interpretation of the area (Figs. 4.3 and 4.5) are shown in Figure 4.1. The interpreted 12-fold surface seismic data displayed in Figures 4.3 and 4.5 were acquired using a source pattern consisting of five 1-kg charges spread over 60 m (at a single shotpoint). The shotpoint location interval was 120 m; the average shot depth was 9 m. The geophone groups consisted of nine in-line 14-Hz geophones over 30 m; the group interval was 30 m. 96 traces were recorded using DFS-V recording equipment and a split-spread geometry. The near offset geophone location was 30 m. The field anti-aliasing filter for the surface seismic was OUT/128 Hz. The surface seismic datum in the area was 1400 m ASL. The refraction statics replacement velocity used to reduce the surface seismic data to the seismic datum was 3350 m/s.

In the initial interpretation, the Leduc reef was interpreted to be fully developed in the area where the VSP-well was drilled. Ultimately, drilling confirmed that the VSP well site was off-reef and that this initial seismic-based interpretation is incorrect.

On the initial interpreted version of the seismic data displayed in Figure 4.3, the northern edge of the Leduc reef is located near trace 242, and full reef is mapped as present at the VSP well site at trace 259. This erroneous interpretation appears to be supported by the patterns of time-structural relief observed along the more prominent seismic events. For example, an event referred to as near-Cambrian event and the Cooking Lake event appear to be pulled up by about 15 ms immediately to the south of trace 242, and the Ireton, Wabamun, Nordegg and Blairmore events appear to drape by up to 25 ms across the interpreted northern edge of the reef. Note that the time-structure at the Blairmore and Nordegg events to the south of trace 314 in Figure 4.3, has been incorrectly attributed to thrust faulting within the Mesozoic section. The time-structure anomaly is seen as the Blairmore Coals and Nordegg events South of trace 290 being shallower in time in comparison to the same events North of trace 290 as a result of the faulting. This misinterpretation is consistent with the regional geology since the Ricinus Field is situated immediately to the east of the line demarcating the eastern limit of the Mesozoic thrust faulting of the Devonian rocks (see Fig. 5 of Moore, 1989a), and structural deformation of varying intensity is observed within the Mesozoic strata in this area.

The geologic section illustrated in Figure 4.4 shows the morphology of the Ricinus Field as interpreted after the drilling of the off-reef VSP well (Hinds et al., 1989a, Hinds et al., 1993c; Hinds et al., 1994c). This geologic section is constrained by well control and is based on the post-VSP interpretation of the example seismic line (Fig. 4.5) and the drilling information description of the geological formations intersected in the VSP borehole. Wells 6-9 and 7-15 (Fig. 4.1) were drilled into a full development of the reef and are productive; 6-9 encountered approximately 22 m of gas pay within the Leduc; and 7-15 encountered 140

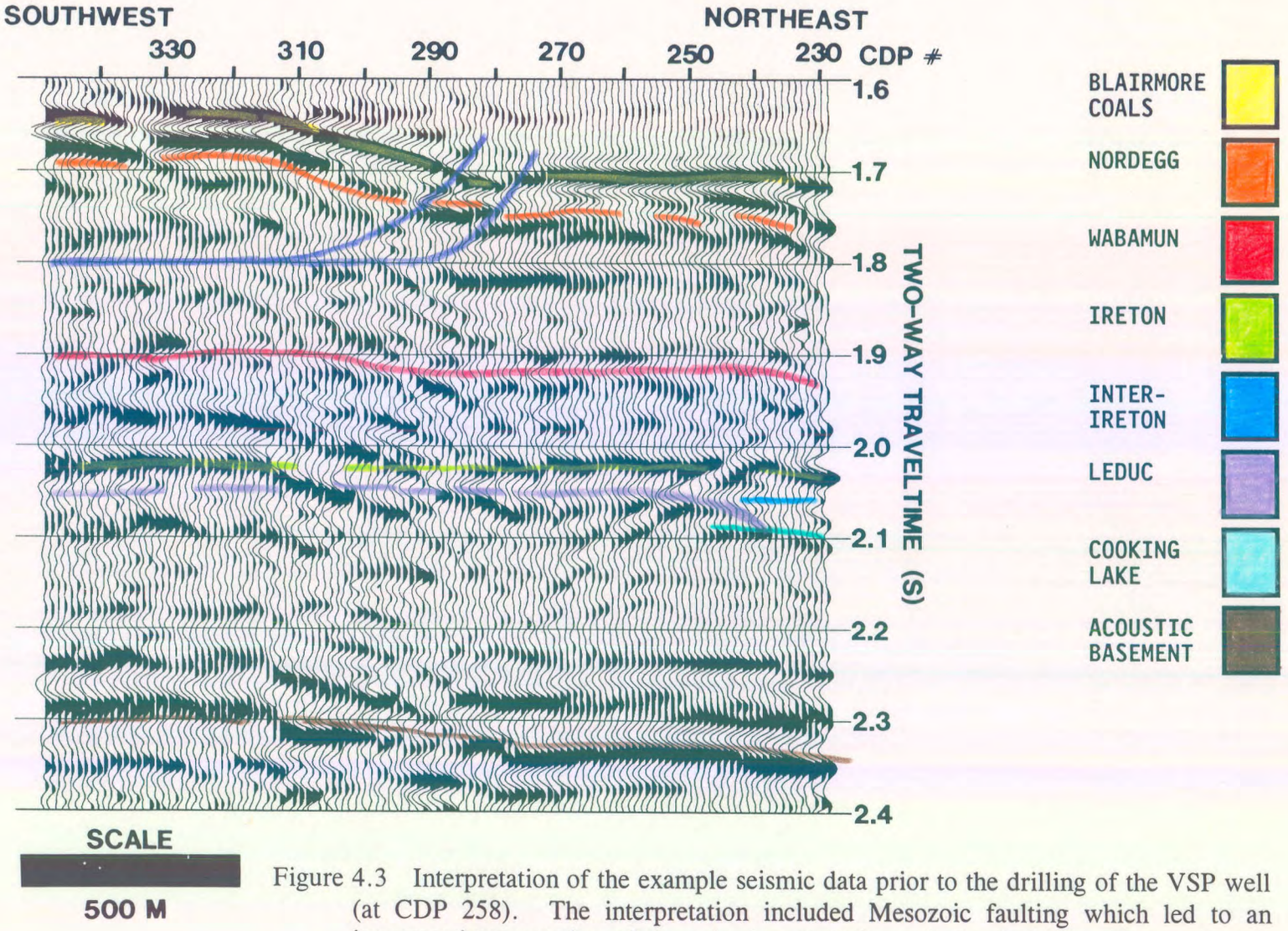

Figure 4.3 Interpretation of the example seismic data prior to the drilling of the VSP well (at CDP 258). The interpretation included Mesozoic faulting which led to an incorrect interpretation of the seismic events beneath the faulting. The preferred, current interpretation is shown in Figure 4.5. The data are normal polarity (from Hinds et al., 1993c; Hinds et al., 1994c).

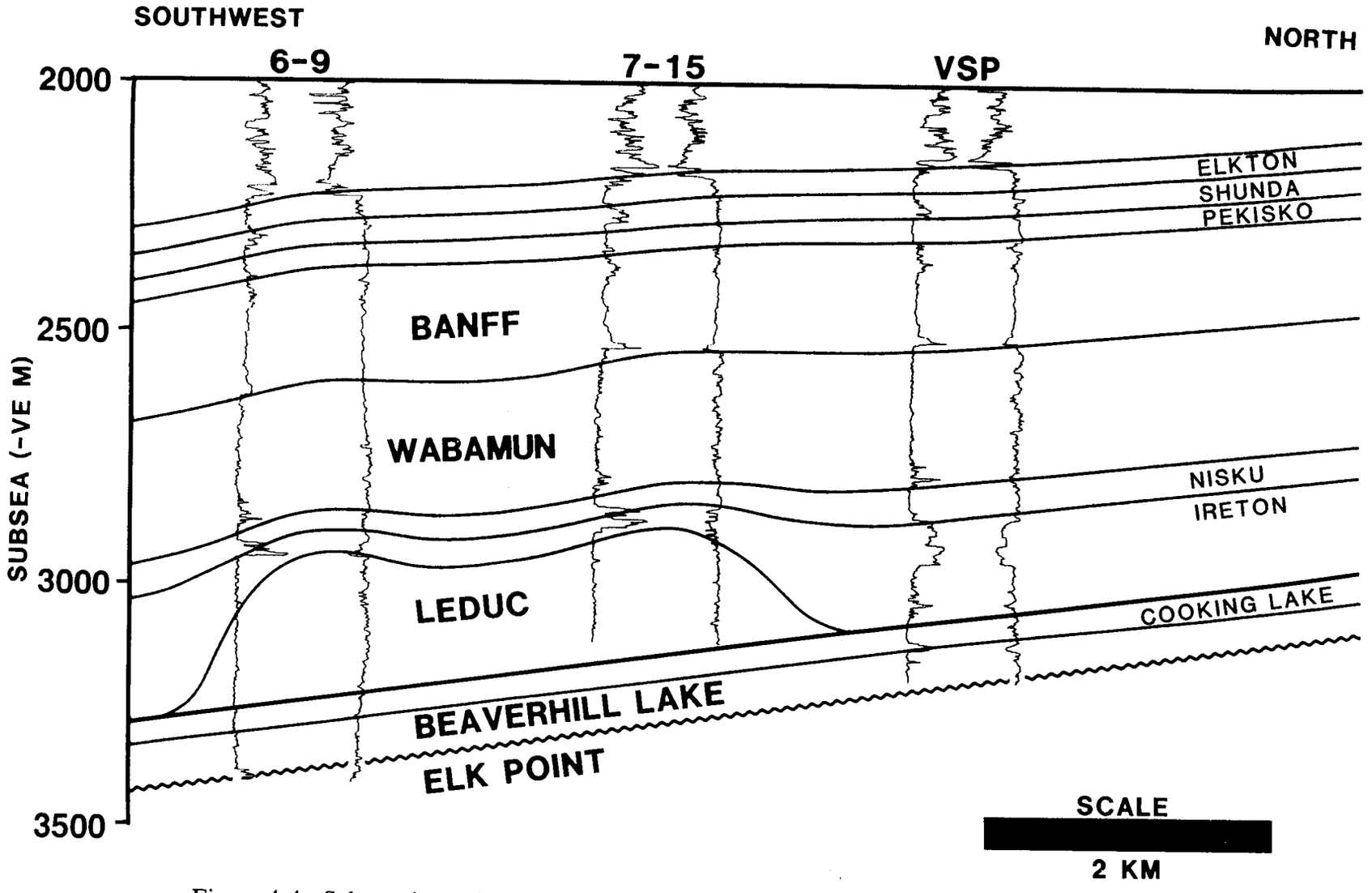

Figure 4.4 Schematic section depicting the subsurface geology at the VSP well site, and the relationships between wells 6-9 and 7-15 (locations shown in Figure 4.1) and the VSP well. The geologic section is consistent with available well log control, and the seismic interpretation displayed as Figure 4.5 (from Hinds et al., 1993c; Hinds et al., 1994c)

m of pay. Well 7-15 penetrated 250 m of Leduc reef. The VSP well (Figs. 4.1 and 4.4) is off-reef, and encountered a full section of inter-reef shale (Ireton and Duvernay; Fig. 3.1A, B and C). Well 6-9 and the VSP well encountered Cooking Lake; however 7-15 was not drilled deep enough to penetrate the Cooking Lake Formation geology.

On the post-VSP well version of the interpretation of the seismic data (Fig. 4.5), the northeastern edge of the Leduc complex is located near trace 314 and the VSP well site (trace 259) is interpreted as off-reef (Hinds et al., 1989a; Hinds et al., 1993c; Hinds et al., 1994c). This interpretation is supported by the patterns of time-structural relief observed along the more prominent seismic events. For example, the acoustic basement event appears to be pulled up by up to 40 ms to the south of trace 314; the Ireton, Wabamun, Nordegg and Blairmore events appear to drape by up to 70 ms across the interpreted northeastern edge of the reef. Note that the time-structural relief observed at the Blairmore coals and Nordegg levels to the south of trace 314, is interpreted as drape and attributed to the differential compaction of reef and off-reef sediment. In this interpretation, Mesozoic thrust faulting has not appreciably affected the rock record (Hinds et al., 1993c; Hinds et al., 1994c).

4.3 VSP data acquisition

After the analysis of the well log data and prior to abandonment, two VSP surveys were run at the VSP well site. These two VSP surveys were designed in an attempt to:

1) more accurately tie the surface seismic to the subsurface geology;

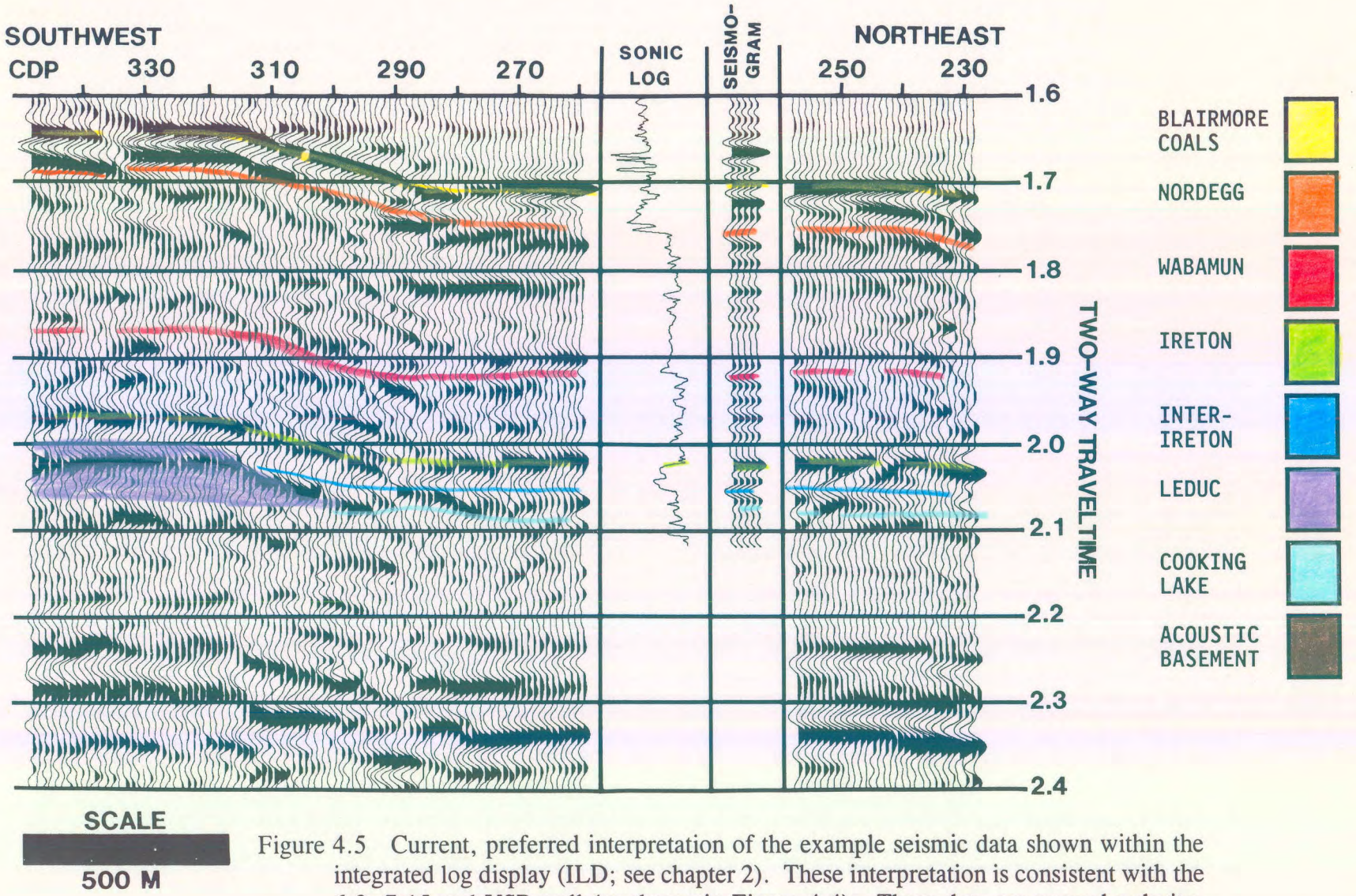

Figure 4.5 Current, preferred interpretation of the example seismic data shown within the integrated log display (ILD; see chapter 2). These interpretation is consistent with the 6-9, 7-15 and VSP well (as shown in Figure 4.4). These data are normal polarity; the display extends from 1.6 s to 2.4 s. The VSP well sonic log (displayed in time) and synthetic seismogram are inserted to display the correlations used in the interpretation (from Hinds et al., 1993c; Hinds et al., 1994c).

2) determine if the reef crest was within 500 m to the Southwest of the VSP well in the direction along the length of the example seismic line with a view to possible whipstocking; and

3) differentiate primary reflections from both surface-generated and interbed multiples.

The near offset source was 199 m from the VSP well and the far offset was 1100 m while both were on-line with respect to the surface seismic line (Fig. 4.1) and in the direction of well 5-22 to the southwest. Two Vibroseis units were operated in series at each offset position. The 16 s sweep ranged from 8 to 80 Hz, the recording length was 20 s, and the cross-correlated output was 4 s. Six to eight sweeps were summed for each geophone sonde location. The SSC 1078 VSP recording system with a sampling rate of 2 ms and a recording filter setting of OUT/OUT was used.

The total depth of the VSP well was 4528 m below KB (KB was 1317 m ASL). The source elevation of both offset source points was 1304 m ASL. Data were recorded at selected depths as the sonde was lowered down the borehole; these sonde locations were repeated during the production run. The use of these dual recording locations facilitates the detection of cable stretch or cable depth counter malfunction, and provides information regarding the gain amplification that will be required during the VSP production run. The first production VSP recording was at 4260 m below KB for the near offset VSP and 4350 m for the far offset VSP survey. During the production recording, the geophone sonde was raised at intervals of 30 m intervals until the depth of 420 m below KB. Above 420 m from the surface (KB), the depth spacing was 60 m up to the shallowest level of 180 m for the zero

offset VSP and 390 m for the far offset VSP. At each sonde location, the three component geophone tool was locked in place.

4.4 Interpretive processing of near offset (199 m) VSP data

During the processing of the near offset VSP, a series of interpretive processing panels were generated to display the following:

1) upgoing and downgoing P-wave separation;

2) deconvolution of the $\mathbf{Z_{up}(+TT)}$ data using an inverse filter calculated from the $\mathbf{Z_{down}(+TT)}$ data; and

3) inside and outside corridor stacks of $\mathbf{Z_{up}(+TT)}$ and $\mathbf{Z_{up(decon)}(+TT)}$ data.

4.4.1 Upgoing P-wave event separation

The separation of upgoing and downgoing P-waves from the **Z(FRT)** data is depicted in the wavefield separation interpretive processing panel (IPP) of Figure 4.6 (Hinds et al., 1989a; Hinds et al., 1993c; Hinds et al., 1994c).

Panel 1 displays the **Z(FRT)** data after trace normalization. In panel 2, these **Z(FRT)** data

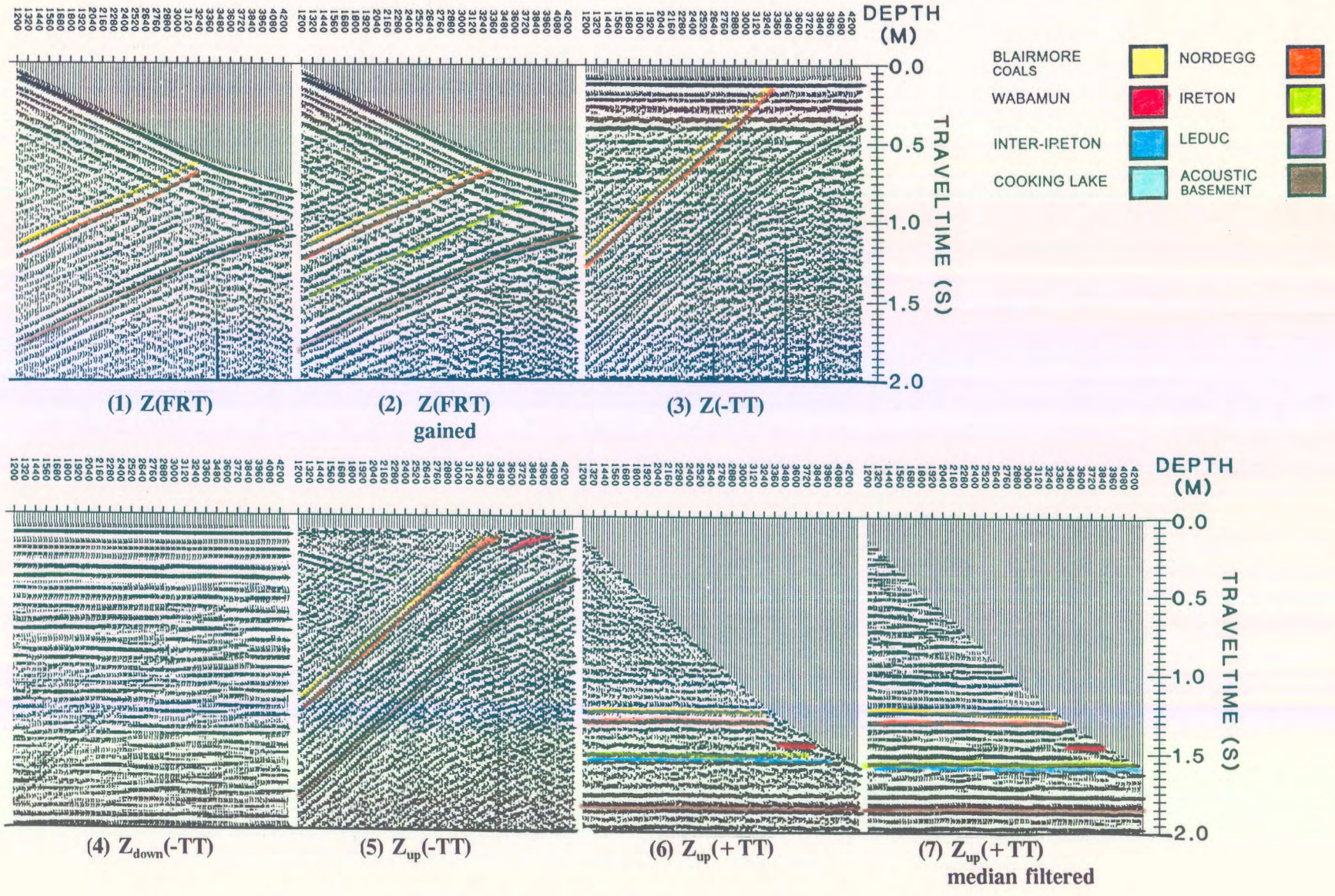

Figure 4.6 Interpretive processing panel depicting the wavefield separation of the near offset VSP data (from Hinds et al., 1989a; Hinds et al., 1993c; Hinds et al., 1994c).

have been gained to highlight several prominent primary upgoing events such as the Blairmore coals, Nordegg, Ireton and acoustic basement (crystalline Precambrian) events. Note that the upgoing event identified as the acoustic basement appears on the 4290 m trace deeper in time than the first break on that trace. Since the event does not intersect the first break curve, the event cannot be positively identified as a primary reflection as reviewed in chapter 1. The uncertainty as to the exact time and depth to crystalline basement cannot be resolved without VSP control at that depth.

The association of the downgoing surface-generated multiple (that lags the first break by approximately 0.3 s) to the upgoing events recorded below TD is bothersome when interpreting the basement reflector. On the **Z(FRT)** data in panel 2, the downgoing multiple event that intersects the deepest trace at 1.05 s coincides with the upgoing wave that begins at 1.05 s and ends on the shallowest trace at 1.65 s. The implication is that some of the events recorded below the bottom may be multiple reflections from the bottom of the borehole itself.

In panel 3 (Fig. 4.6), the **Z(-TT)** data are presented where the first breaks and downgoing P-wave multiple events are horizontally aligned. The **Z(-TT)** data in panel 3 illustrate that the downgoing wavetrain consists of the primary downgoing wavelet plus high-amplitude surface-generated multiples and less prominent possible interbed multiples. The surface-generated downgoing multiples are recognized as those horizontally aligned, post-first break arrivals that are recorded on all of the traces. As reviewed in chapter 1, if a downgoing multiple event does not extend over the entire depth range but is evident on the deeper traces only, then that multiple is interpreted to be an interbed multiple (Hinds et al., 1989a).

In the next processing step, an 11-point median filter was used to remove the upgoing P-waves. The output consisted of separated and scaled $\mathbf{Z_{down}(-TT)}$ data and is displayed in panel 4. Note that the residual upgoing wave content in the $\mathbf{Z_{down}(-TT)}$ data is minimal. This panel is one of the most important panels for interpretive processing of VSP data. If residual upgoing events remain in the $\mathbf{Z_{down}(-TT)}$ data, then that amount of residual upgoing event is subtracted out of the **Z(-TT)** data (panel 3) during wavefield separation.

The multiples that appear on all of the traces are most likely surface-generated. This is the case for multiples down to 0.45 s. Beyond that time on panel 4, surface generated and interbed multiples (as seen between 0.75 and 0.9 s) exist.

In the next step of the wavefield separation, the $\mathbf{Z_{down}(-TT)}$ data of panel 4 were subtracted from the **Z(-TT)** in panel 3 to yield the output $\mathbf{Z_{up}(-TT)}$ data shown in panel 5. The upgoing P-waves and downgoing shear waves (both primary and multiples) are shown in panel 5. The downgoing shear waves (SV) may have been generated at the bottom of the surface casing or near the surface. An example of a downgoing SV appears on the shallowest trace on panel 5 at 0.2 s (**-TT** time) and trends opposite to the upgoing events (deeper in time from left to right).

The $\mathbf{Z_{up}(+TT)}$ before and after the application of a 3-point median filter are shown in panels 6 and 7, respectively. The equalized amplitudes of the horizontally aligned upgoing waves for the Blairmore coals, Nordegg, Wabamun, Ireton, inter-Ireton, Cooking Lake, and acoustic basement events are interpreted in panel 7. It can be observed that the downgoing SV events seen in panel 5 dip more steeply in the **+TT** display; however, these events have

been effectively attenuated by the application of the median filter. As will be discussed further below, the Wabamun and Cooking Lake events have been identified only on traces deeper than the depth of the Nordegg interface due to multiple interference.

4.4.2 VSP deconvolution

On the $\mathbf{Z_{down}(-TT)}$ data, as reviewed in chapter 1, the initial downgoing pulse (except in the case of head wave contamination) is the primary downgoing P-wave; any later arriving, downgoing events are multiples (apart from downgoing shear or converted waves). Ideally, P-wave multiples can be effectively filtered using a deconvolution operator derived from an analysis of the separated downgoing P-wave wavetrain (Hardage, 1985; Hinds et al., 1989a). Deconvolution also enhances the higher frequencies within the data which allows for better vertical resolution.

The deconvolution IPP shown in Figure 4.7 (Hinds et al., 1989a; Hinds et al., 1993c; Hinds et al., 1994c) was designed to enable the monitoring of the deconvolution process of the Ricinus $\mathbf{Z_{up}}$ data. The incorporated panels reveal information (about multiples) that was difficult to determine from the wavefield separation IPP (Fig. 4.6) alone. The first two panels (Fig. 4.7) are the nonfiltered and median-filtered $\mathbf{Z_{up}(+TT)}$ data, respectively. Panel 3 contains the **Z(-TT)** data which allows an examination of the downgoing P-wave multiple pattern of the near offset data. Panels 4 and 5 contain the $\mathbf{Z_{up}(-TT)}$ and $\mathbf{Z_{up(decon)}(-TT)}$ data,

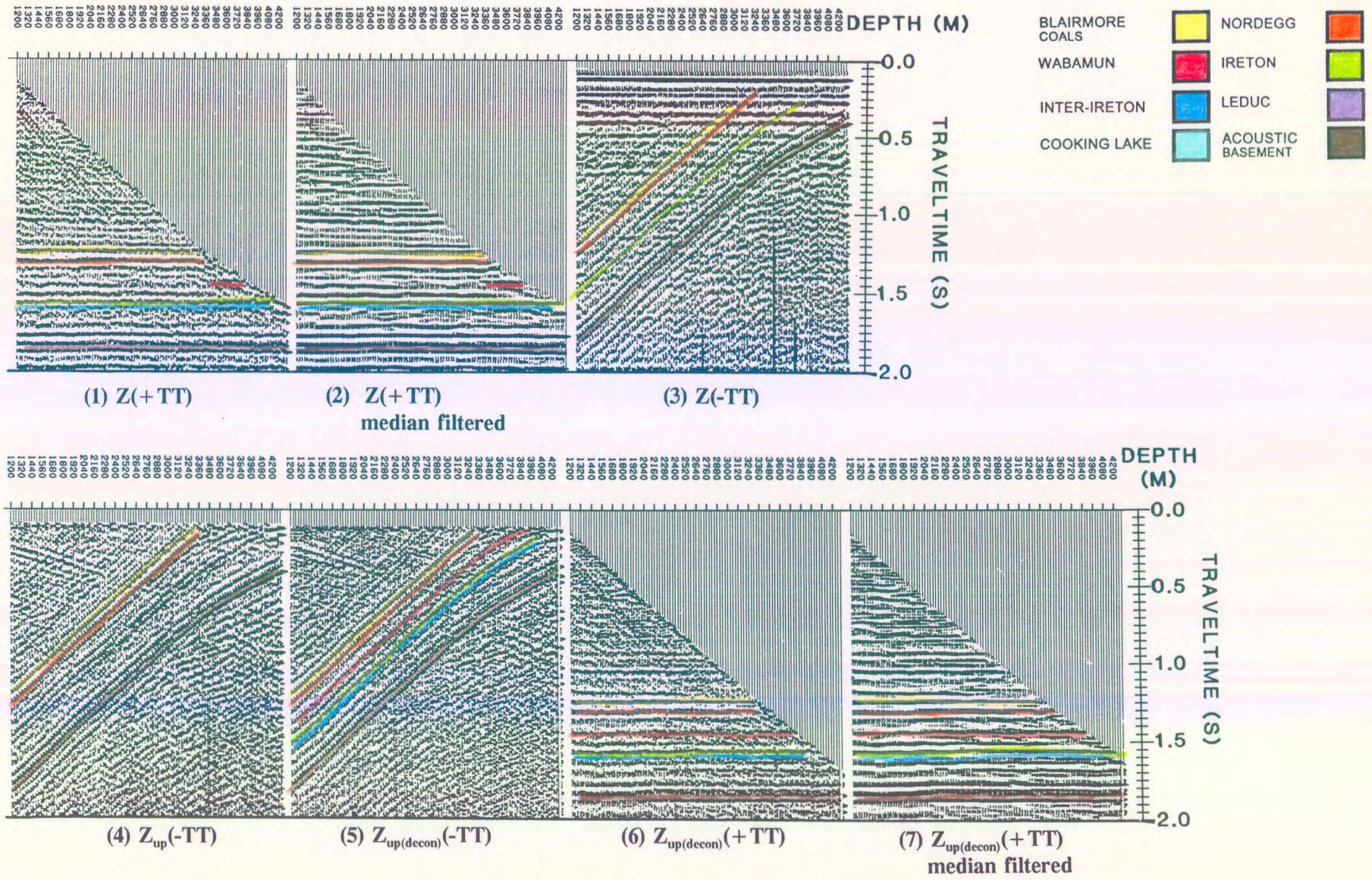

Figure 4.7 Interpretive processing panel depicting the deconvolution of the near offset VSP data (from Hinds et al., 1989a; Hinds et al., 1993c; Hinds et al., 1994c).

respectively. Both panels 4 and 5 are contaminated with downgoing shear waves. The downgoing SV events can be recognized by the observation that the events increase in traveltime with increasing depth and penetrate the upgoing events that decrease in traveltime with increasing depth. A comparison of these panels illustrates that the deconvolution process has enhanced the higher frequencies contained in the upgoing waves and preserved the primary reflections yet has not raised the noise content of the data.

The last two panels (6 and 7) contain the nonfiltered and median-filtered $\mathbf{Z_{up(decon)}(+TT)}$ data, respectively. A comparison of panels 2 and 7 (Fig. 4.7), elucidates the effect of the Blairmore coals and Nordegg multiples on the continuity of primary reflections. Multiple contamination is most noticeable for the Wabamun and Cooking Lake reflection events. On the $\mathbf{Z_{up}(+TT)}$ data in panel 2, the Wabamun is relatively unaffected on traces that are recorded below the Nordegg depth of 3466 m (-2151 m ASL). The upgoing multiple reflection from the Nordegg will not be detected on traces deeper than the bottom-generating layer of the multiple (the Nordegg) because, by definition, the multiple is an upgoing wave, not downgoing. Examination of panel 3 reveals that a series of possible surface-generated multiples exist (a series of events parallel to the first break primary (**-TT**) that are delayed in time). The multiple contamination may persist for 0.4 s or more. It is likely that both surface-generated and interbed multiples may be contaminating the $\mathbf{Z_{up}(+TT)}$ data at the Wabamun event time level. On traces recorded at depths shallower than 3466 m, the multiple events generated at the Nordegg Formation interface destructively interferes with the Wabamun event.

A trough interpreted to be the Cooking Lake event is just below the inter-Ireton trough in

panel 2 ($\mathbf{Z_{up}(+TT)}$ data) on the traces from depth 3466 m to the bottom of the borehole. The interpretation of the Cooking Lake event (Hinds et al., 1993c) is supported by the sonic log/synthetic seismogram Cooking Lake correlation to the surface seismic (ILD) shown in Figure 4.5 (the sonic log was integrated to create a synthetic seismogram and corrected using the VSP first break times). What effect does deconvolution have on the Wabamun and Cooking Lake events?

An investigation of the effect that deconvolution has on the Wabamun and Cooking Lake events shows that the Wabamun event is now laterally continuous on the $\mathbf{Z_{up(decon)}(+TT)}$ data in panel 7 (Fig. 4.7) and can be correlated on all depth traces as a result of the deconvolution. The Cooking Lake event (trough) can also now be confidently interpreted since the event is now a recognizable event across the entire $\mathbf{Z_{up(decon)}(+TT)}$ data.

The multiple contamination is interpreted to be minimal in the zone of interest around the Ireton event. The inter-Ireton is continuous and does not exhibit significant structure either before or after the VSP deconvolution. It is the inter-Ireton event that will rise and/or truncate against any Ricinus reef edge and is therefore regarded as a vital key to the interpretation success of the VSP surveys (Hinds et al., 1993c).

4.4.3 Inside and outside corridor stacks

Inside and outside corridor stacks (Hinds et al., 1989a) and associated displays for the nondeconvolved $\mathbf{Z_{up}(+TT)}$ data are presented in Figure 4.8. A comparison of the $\mathbf{Z_{up}(+TT)}$ outside and inside corridor stacks (panels 3 and 4, respectively) illustrates the utility of these displays. For example, the multiple interference generated by the Blairmore coals or Nordegg interbed multiple can be interpreted on the inside corridor stack but is not seen on the outside corridor stack. On the $\mathbf{Z_{up}(+TT)}$ data outside corridor stack in panel 3, the Wabamun trough dominates (at 1.85 s); however the $\mathbf{Z_{up}(+TT)}$ data inside corridor stack at the same time window shows no semblance of a Wabamun event. This is due to multiple interference that has destructively interfered with the Wabamun event on the depth traces shallower than the Nordegg primary (the same depth trace range that the Nordegg multiples must exist on; Hinds et al., 1989a; Hinds et al., 1993c; Hinds et al., 1994c).

On the unmuted input data for the corridor stack displays (Figure 4.8, panels 1 and 6), it can be noted that the Cooking Lake event exists as a trough beneath the inter-Ireton event (trough). The event is so weak without the deconvolution that even the outside corridor stack does not show the Cooking Lake trough. This indicates the reason for displaying the unmuted input data in the corridor stack IPP during interpretive processing (Hinds et al., 1989a). In order to interpret the outside corridor stack, it must be borne in mind what went into the stack (where the corridor mute line is).

On the $\mathbf{Z_{up(decon)}(+TT)}$ data corridor stack panels of Figure 4.9, the Wabamun and Cooking Lake events can now be reliably interpreted.

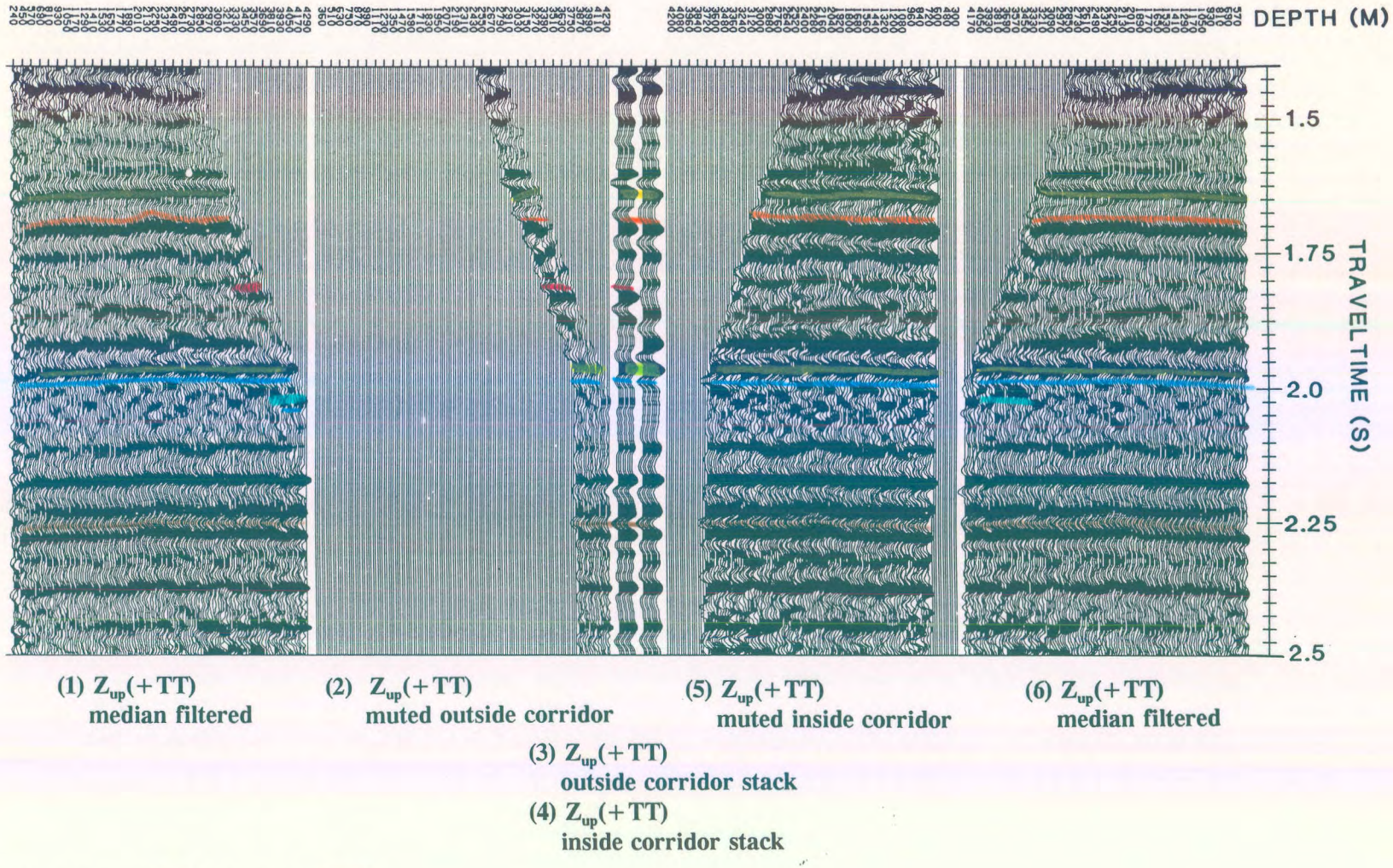

Figure 4.8 Interpretive processing panel illustrating the utility of the nondeconvolved inside and outside corridor stacks for the Ricinus near offset $Z_{up}(+TT)$ data (from Hinds et al., 1989a; Hinds et al., 1993c; Hinds et al., 1994c).

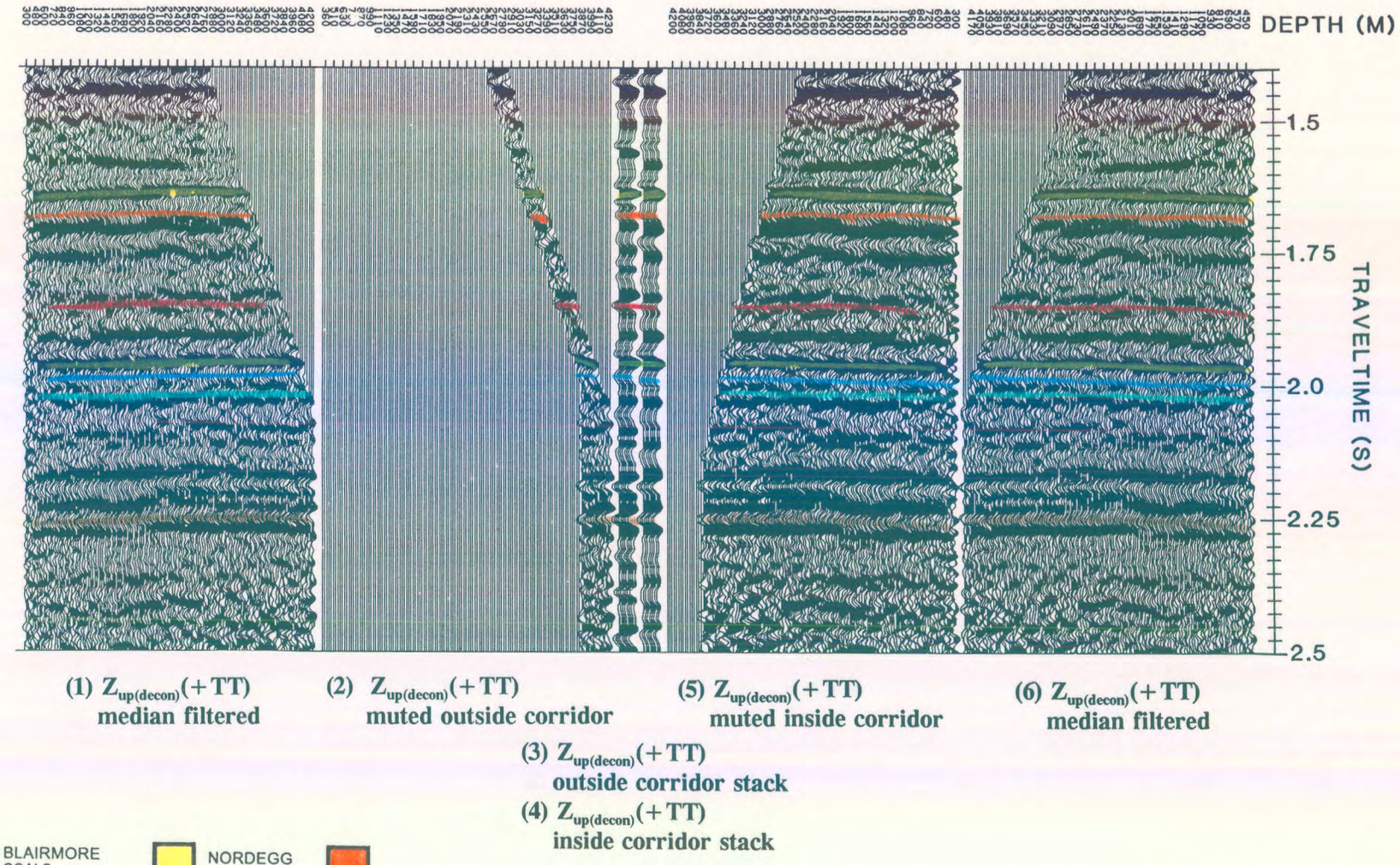

Figure 4.9 Interpretive processing panel illustrating the utility of the deconvolved inside and outside corridor stacks for the Ricinus near offset $Z_{up(decon)}(+TT)$ data (from Hinds et al., 1989a; Hinds et al., 1993c; Hinds et al., 1994c).

If deconvolution is successful, the $\mathbf{Z_{up(decon)}(+TT)}$ outside and inside corridor stacks (panels 3 and 4; Fig. 4.9) should be similar. The inside and outside deconvolved corridor stacks show that the surface generated multiples have been substantially attenuated by the VSP deconvolution process; however there is enough difference (as in the zone immediately below the Nordegg event at about 1.75 to 1.8 s) between the events of the two stacks to predict that any possible interbed multiples have been simply attenuated but not totally removed.

The deconvolved data and the corridor stacks show that the Wabamun and Cooking Lake primaries are flat lying continuous upgoing primary events across the entire VSP panel once the effect of multiple contamination is minimized. At this point the surface seismic can be reinterpreted at the well location by making use of the VSP results.

4.5 Interpretive processing of the far offset (1100 m) VSP data

On the far offset VSP data, the vertical (**Z**), and both horizontal (**X** and **Y**) axis contain nonpartitioned elements of the upgoing and downgoing P- and SV-wavefields. Examination of the IPPs to follow will reveal that the partitioning of the wavefields (both up- and downgoing P and SV events) has significant implications with respect to interpretation. In chapter 2, the Ricinus far offset data was utilized as an example of a problematic VSP data for interpretive processing. It was these data that showed how interpretive processing aided in the searching out of the origins of the problematic "noise" wavefields within the example far offset data. In this section, the interpretive processing will be shown in more detail. The reader is referred to chapter 2 with regards to the difference in runstream approaches.

As demonstrated in panels 5 and 6 of the near offset wavefield separation IPP (Fig. 4.6), a downgoing SV wave (trending in the opposite direction to the upgoing waves in panel 5) is noticeable. Normally, downgoing and upgoing shear waves are not seen on near offset data. The near offset surveys usually contain events resulting from near-vertical incidence reflections. From Zoeppritz equations, the partitioning of downgoing P waves into up- and downgoing SV waves should be minimal under conditions of near-vertical incidence reflections. It can therefore be expected that shear wave contamination will be readily noticeable on the far offset data. The runstreams used for the partitioning of the wavefields presented below will play an important role in isolating the upgoing P wave events from downgoing P wave events and up- and downgoing SV events. As illustrated in chapter 2, interpretive processing is used to assist in the modification of the processing runstreams.

Far offset IPPs have been designed to control the quality of execution of the following procedures:

1) hodogram-based rotation of the **X**, **Y**, and **Z** data (based on windowed data enveloping the P-wave first arrival; DiSiena et al., 1984, Hinds et al., 1989a);

2) time-variant model-based rotations applied to the $\mathbf{HMAX_{up}(FRT)}$ and $\mathbf{Z_{up}(FRT)}$ data in response to interpretive processing results as highlighted in chapter 2 (within the section "problematic far offset interpretive processing"); and

3) the VSP-CDP mapping of the data (Dillon and Thomson, 1984).

4.5.1 Hodogram-based rotation

The **X(FRT)**, **Y(FRT)**, and **Z(FRT)** data for the far offset VSP are displayed in Figure 4.10 as panels 1, 2, and 3, respectively. The **X(FRT)** and **Y(FRT)** data contain both P and SV downgoing waves plus recognizable upgoing SV events. These upgoing SV events can be seen on both panels 1 and 2 originating at depth levels 2790 down to the deepest traces (coloured purple in panels 1 and 2). More upgoing SV events may exist originating on the shallower traces but are overpowered in amplitude by the downgoing mode-converted SV events. The **HMAX(FRT)** data in panel 5 shows a clear definition of the up- and downgoing SV events. These events (coloured pink in panels 5 and 6) slope differently to the upgoing P wave events of the **Z(FRT)** data seen on panel 3.

The partitioned downgoing primary P waves (first breaks wavelet) are consistent on both the **X(FRT)** and **Y(FRT)** data in panels 1 and 2 on traces recorded in the upper two-thirds of the borehole which may indicate that the tool was rotating on the deeper depth traces (indicated by the first breaks becoming inconsistent on a single panel). In panel 3, the **Z(FRT)** data first breaks are phase consistent.

The hodogram-based rotation of the **X(FRT)** and **Y(FRT)** data onto the **HMIN(FRT)** and **HMAX(FRT)** data is illustrated using panels 1, 2, 4 and 5, respectively. This rotation corrects for first break inconsistencies due to the rotation of the tool during the movement of the sonde up the borehole by projecting data from both of the input channels onto an axis which lies in the plane defined by the borehole and the source; namely the **HMAX(FRT)** data. **HMIN(FRT)** and **HMAX(FRT)** data are assumed to be aligned perpendicular to and

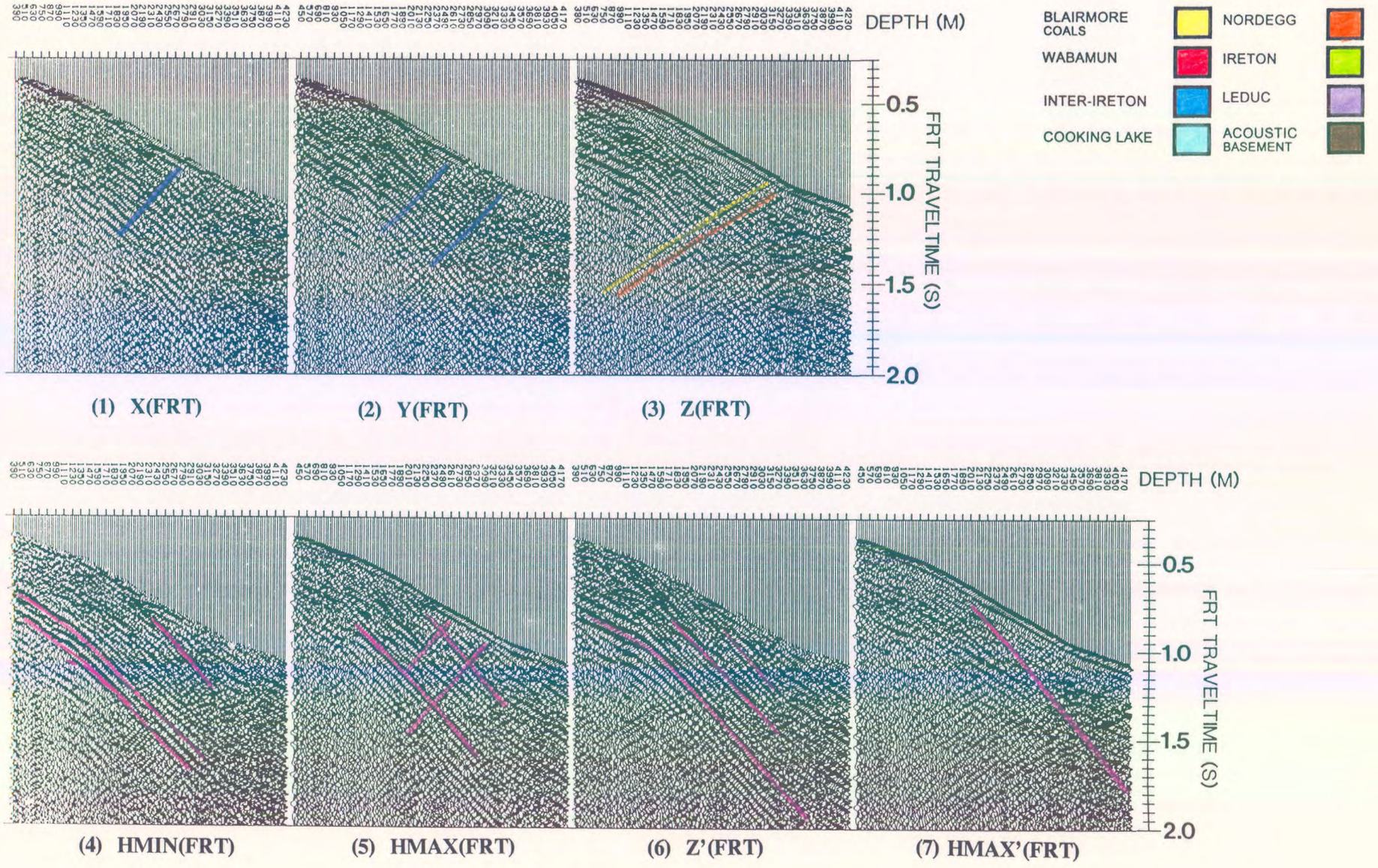

Figure 4.10 Interpretive processing panel depicting the hodogram-based rotation of the far offset Ricinus VSP data (from Hinds et al., 1989a; Hinds et al., 1993c; Hinds et al., 1994c).

in the plane formed by, the source and wellbore, respectively. Note that the **HMIN(FRT)** data (comprised of horizontally polarized shear (SH) wave events and out of the plane reflections), contains possible downgoing SV waves (coloured pink in panel 4 and appearing on the shallow traces below 0,6 s) that could originate at the casing joints or reflected downgoing waves that originate from out of the plane of the well.

The remnant of a mode-converted downgoing SV wave with components within the **HMIN(FRT)** data appears at the Nordegg and Blairmore level. The upgoing SV events from the Nordegg and Blairmore coals that were first noticed on both of the **X(FRT)** and **Y(FRT)** data are now more noticeable after redistribution onto the **HMAX(FRT)** data. These two upgoing SV events are coloured purple on panel 5. Unfortunately, the downgoing SV events on the **HMAX(FRT)** data are of equal amplitude to the downgoing P waves. The **HMAX(FRT)** data contains consistent polarized downgoing P wave first breaks as the data of the input **X(FRT)** and **Y(FRT)** channel data have been rotated into the plane containing the downgoing P wave.

The **Z'(FRT)** data in panel 6 and the **HMAX'(FRT)** data in panel 7 were obtained by rotating the **Z(FRT)** and **HMAX(FRT)** data using polarization angles estimated from a hodogram analysis of data within a window around the P-wave first arrival (DiSiena et al., 1984; Hinds et al., 1989a). This technique is designed to polarize the data so that the downgoing P-waves are effectively isolated on a single channel, **HMAX'(FRT)**.

On the **HMAX'(FRT)** data in panel 7 of Figure 4.10, the downgoing P-wave energy is

dominant. The **HMAX'(FRT)** panel contains residual downgoing shear (SV) waves (converted to SV waves at the Blairmore coal interface) and upgoing P-wave energy. This indicates that the polarization required to delineate the downgoing P-wave data onto a single panel is not adequate to separate the upgoing P-wave data entirely onto the orthogonally aligned **Z'(FRT)** data.

The **Z'(FRT)** data shown in panel 6 contains downgoing shear wave (coloured pink in panel 6) and upgoing P-wave energy that fit the assumption that the primary upgoing P-waves are orthogonal to the primary downgoing P-waves (isolated on the **HMAX'(FRT)** data). The downgoing shear wave overshadows the lower amplitude upgoing P-wave. The time-variant polarization of the data (modelled on the upgoing P-waves) should attempt to detach the contaminating up- and downgoing shear waves from the upgoing P-waves and isolate interpretable upgoing P-wave events onto a single output data panel, **Z"$_{up}$(FRT)**; however, it will be shown that this "routine-type" processing does not produce optimal results for interpretation and that a modified processing runstream is necessary (Hinds et al., 1994c).

4.5.2 Time-variant model-based rotation

The normal time-variant rotation runstream recommended in chapter 2 was used for the Ricinus far offset data and the resulting time-variant polarization IPP (Hinds et al., 1989a; Hinds et al., 1994c) is shown in Figure 2.50 and interpreted in Figure 4.11. As concluded in that example processing the **Z"$_{up}$(FRT)** data (in panel 6 of Figs. 2.50 and 4.11) contained unacceptable amounts of diffraction and mode-converted SV up- and downgoing events.

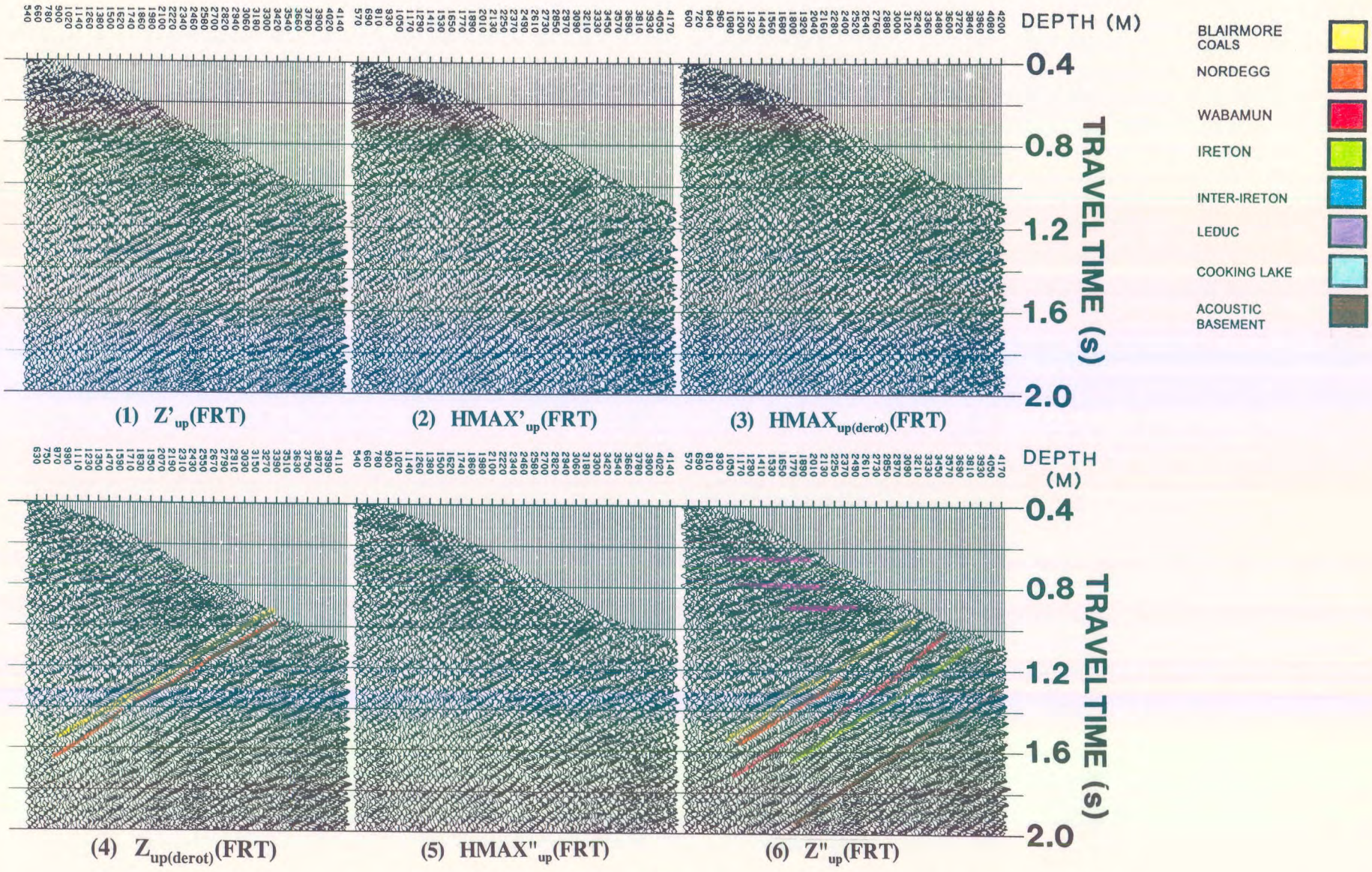

Figure 4.11 Interpretive processing panel depicting the time-variant model-based rotation of the far offset Ricinus VSP data resulting from the suggested processing runstream in chapter 2 (from Hinds et al., 1989a; Hinds et al., 1993c; Hinds et al., 1994c).

The time-variant model-based polarization runstream (as suggested in chapter 2) was changed to eliminate the second polarization rotation and to begin the runstream that eventually outputs the **Z"$_{up}$(FRT)** data by performing wavefield separation on the **Z(FRT)** and **HMAX(FRT)** data. The **HMAX'(FRT)** data displayed in Figure 4.10 were retained for the far offset deconvolution trials presented in chapter 2 and reviewed later in this chapter. The modified interpretively processed time-variant model-based polarization results are shown in Figure 4.12.

The **HMAX(FRT)** and **Z(FRT)** data (panels 1 and 2) are wavefield separated using the F-K based surgical muting (see chapter 2) to output the **HMAX$_{up}$(FRT)** and **Z$_{up}$(FRT)** data shown in panels 3 and 4, respectively. Special emphasis within the F-K mute design was taken to also attenuate the up- and downgoing SV-events from both input panels. The lack of the second hodogram-based rotation on the **Z(FRT)** and **HMAX(FRT)** input data (used in the wavefield separation) eliminated the possibility of rotation induced noise.

These data (panels 3 and 4 of Fig. 4.12) are compared to the final two panels (5 and 6) containing the time-variant model-based polarized **HMAX"$_{up}$(FRT)** and **Z"$_{up}$(FRT)** data. The emphasis is on the improvement of the quality of the upgoing P-wave events on the **Z"$_{up}$(FRT)** panel and the similar **Z"$_{up}$(FRT)** resulting from the use of the normal processing runstream (without interpretive processing) as shown in Figure 4.11. The upgoing events on panel 6 of Figure 4.12 are easily interpretable; however the same events on panels 5 and 6 of Figure 4.11 are difficult to interpret due to interfering noise. The updated **Z"$_{up}$(FRT)** does contain residual diffraction events (between 0.7 and 0.9 s and coloured pink) which manifest themselves as horizontal events.

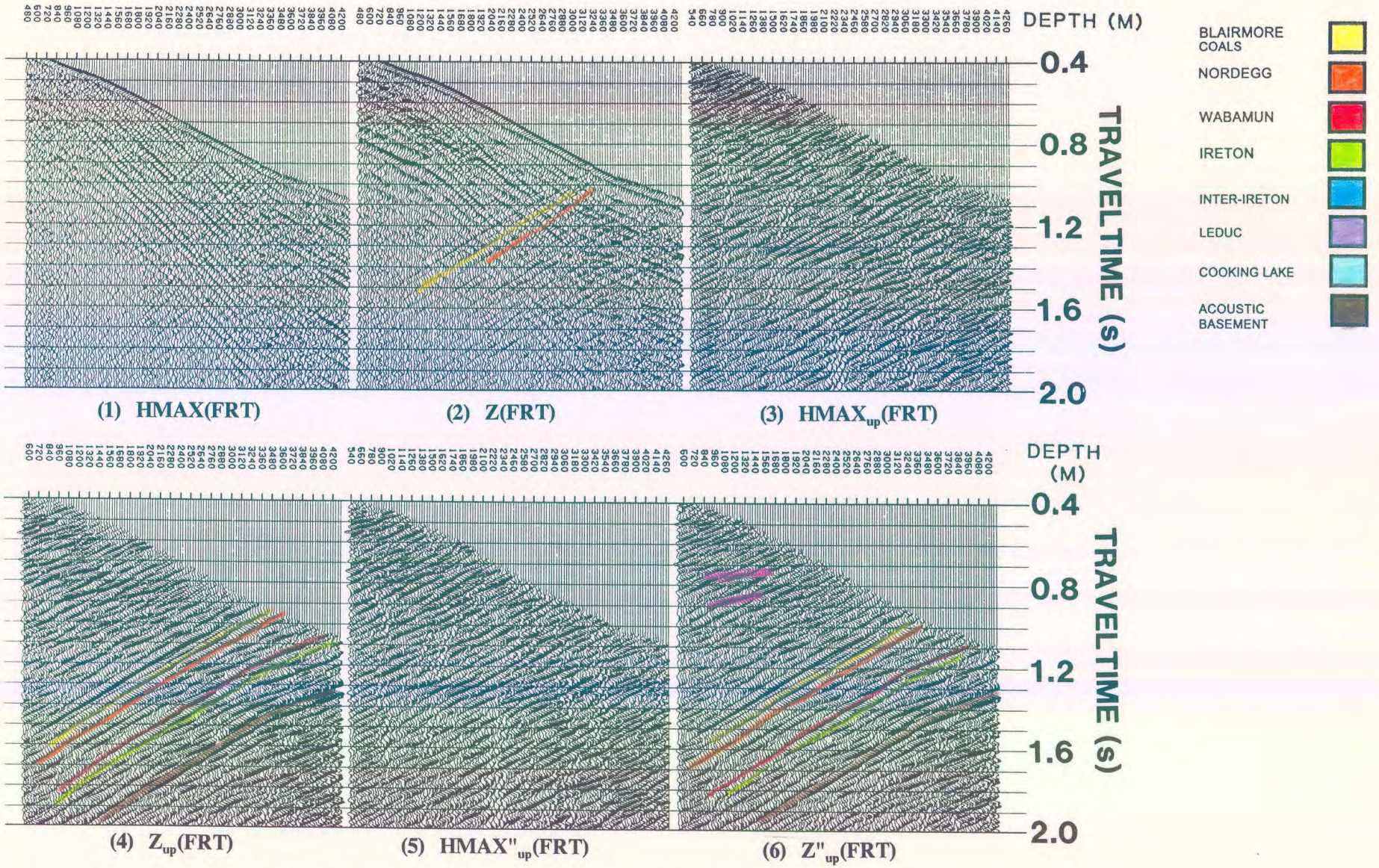

Figure 4.12 Interpretive processing panel depicting the time-variant model-based rotation of the far offset Ricinus VSP data resulting from interpretive processing (from Hinds et al., 1989a; Hinds et al., 1993c; Hinds et al., 1994c).

On the $\mathbf{Z_{up}(FRT)}$ data in panel 4 of Figure 4.12, upgoing P-waves generated by shallow reflectors are improperly aligned (due to the choice of non-time variant rotation angles). The deeper events do not suffer much misalignment because deep event raypath geometries satisfy the near-vertical incidence angle assumption better than the raypaths of shallower events. The time-variant model-based rotation corrects for this misalignment of the shallow events. The output upgoing wave displays, $\mathbf{HMAX''_{up}(FRT)}$ and $\mathbf{Z''_{up}(FRT)}$, are shown on panels 5 and 6 in Figure 4.12, respectively. Note that the shallow events display better alignment than on the $\mathbf{Z_{up}(FRT)}$ in panel 4. The rotation angle required for the Blairmore coals event on a particular trace was different to the rotation angle for deeper events (such as the acoustic basement) on the same trace. The time-variant rotation technique (Hinds et al., 1989a) generated these different rotation angles.

4.5.3 Deconvolution of the far offset data

The most realistic approximation to a far offset VSP deconvolution uses the separated polarized downgoing waves, $\mathbf{HMAX'_{down}(-TT)}$, and the separated time-variant polarized upgoing P-waves contained in the $\mathbf{Z''_{up}(FRT)}$ data, shown in panel 6 of Figure 4.12. To illustrate the deconvolution, a far offset deconvolution IPP to assist in the evaluation of the effect of far offset deconvolution on the $\mathbf{Z''_{up}}$ data (Figs. 2.56 and 4.13) has been designed. The deconvolution process involved designing the inverse wavelet for the $\mathbf{HMAX'_{down}(-TT)}$ data (panel 2 of Fig. 4.13) and subsequently applying the operator to the $\mathbf{Z''_{up}(-TT)}$ data (panel 4 of Fig. 4.13).

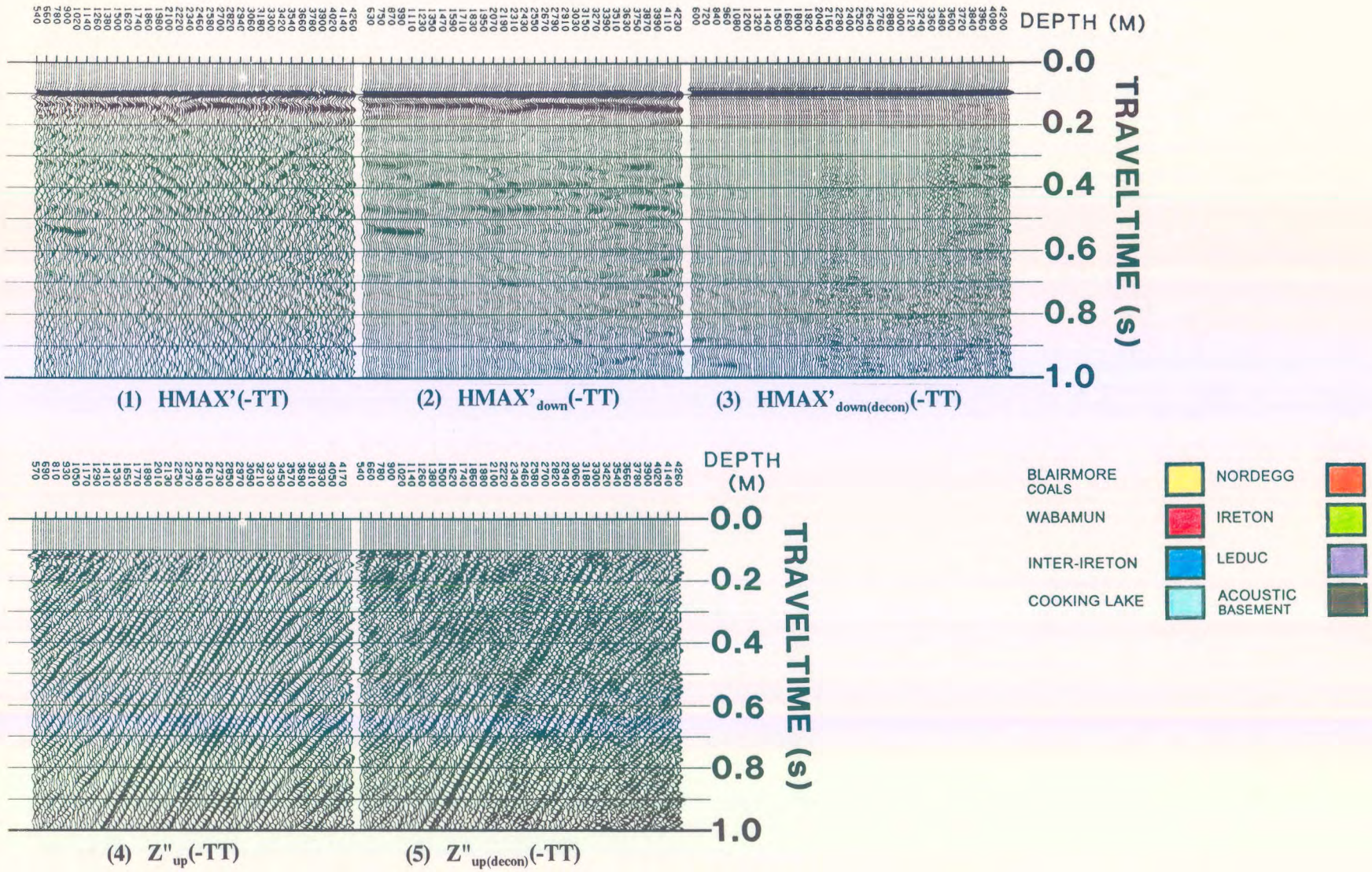

Figure 4.13 Interpretive processing panel depicting the far offset deconvolution of the Ricinus VSP data (from Hinds et al., 1993c; Hinds et al., 1994c).

The deconvolution was performed on the **Z"$_{up}$(-TT)** far offset data (see Figs. 2.56 and 2.57); however the process added unacceptable noise to the data. This can be seen by comparing the **Z"$_{up}$(-TT)** and **Z"$_{up(decon)}$(-TT)** data shown in panels 4 and 5 in Figure 4.13. The upgoing P-wave events have become difficult to interpret on the deconvolved data.

In the final interpretation, the non-deconvolved far offset VSP data was evaluated to contain minimal multiple contamination at the zones of interest on the **Z"$_{up}$(+TT)** data (on the Blairmore Coals down to the Acoustic Basement events shown in panel 6 of Fig. 4.12). For the far offset VSP data, the Blairmore or Nordegg multiples have a longer travel path to reach the Wabamun in comparison to the near offset VSP data. The Wabamun seems to be less affected on the far offset VSP data by the Blairmore coal or Nordegg multiple than on the near offset VSP data for this reason. This results in the deconvolution process for the far offset VSP data becoming a non-necessary step in the far offset processing runstream for this data.

4.5.4 VSP-CDP mapping

The **Z"$_{up}$(+TT)** data from panel 6 of Figure 4.12 are used for the interpretation of the off-reef markers. Two interpretation panels are used for this purpose. The first focuses on the transformation of the **Z"$_{up}$(+TT)** data in time (**+TT**) and depth into the VSP-CDP (Dillon and Thomson, 1984) domain of time (**+TT**) and offset distance from the well. The interpretive processing of the VSP-CDP mapping is displayed in the VSP-CDP IPP of Figure 4.14. For comparison, the VSP-CDP IPPs resulting from the normal time-variant runstream

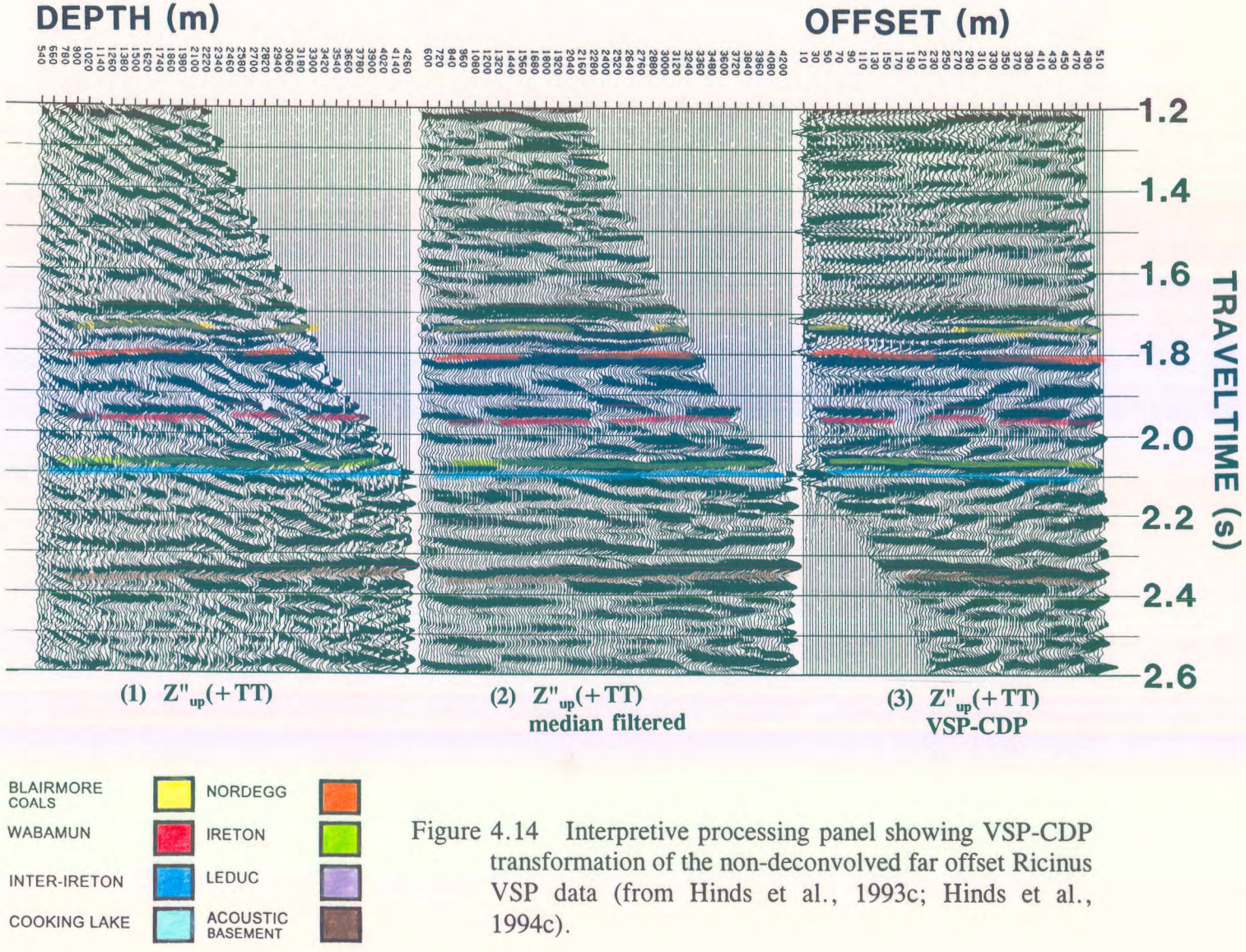

Figure 4.14 Interpretive processing panel showing VSP-CDP transformation of the non-deconvolved far offset Ricinus VSP data (from Hinds et al., 1993c; Hinds et al., 1994c).

suggested in chapter 2 and from the far offset deconvolution are presented in Figures 4.15 and 4.16, respectively. The second interpretation panel is the integrated seismic display shown in Figure 4.17 of the merged VSP-CDP display and the surface seismic data.

The **Z"$_{up}$(FRT)** data in panel 6 of Figure 4.12 placed in **+TT** time are shown as the first panel of the VSP-CDP IPP in Figure 4.14. A median filtered **Z"$_{up}$(+TT)** and the VSP-CDP mapped data (pseudo-two-way traveltime versus offset) are shown as panels 2 and 3, respectively.

The Blairmore coals, Nordegg, Wabamun, Ireton, inter-Ireton, Cooking Lake and acoustic basement markers are interpreted on these presentations. The median filtering (panel 2) as well as the VSP-CDP mapping processing (panel 3) have not appreciably distorted the interpretability of the original data (**Z"$_{up}$(+TT)** data in panel 1 of Fig. 4.14).

The Ireton and inter-Ireton events are interpreted to be continuous and effectively parallel indicating that only off-reef events (as opposed to reefal events) have been imaged on the far offset VSP data. In contrast, the displays in Figures 4.15 and 4.16 are difficult to interpret in comparison to the data in Figure 4.14 because of the interfering noise and deconvolution processing artifacts. Interpretive processing improved the original mode-converted up- and downgoing SV-contaminated **Z$_{up}$(FRT)** and **HMAX$_{up}$(FRT)** data sufficiently enough (as shown in the final results of Fig. 4.14) to enable a confident interpretation during each processing step.

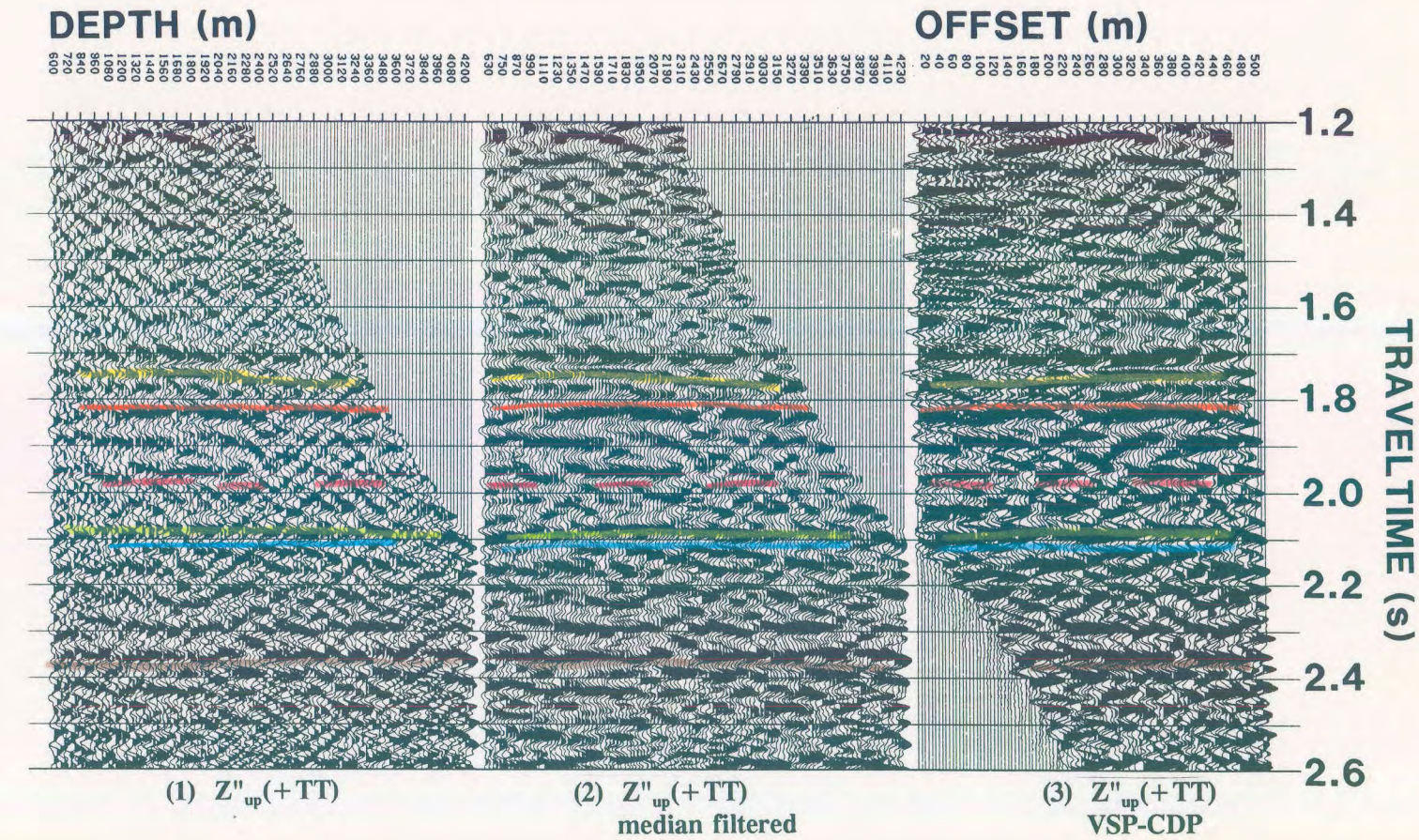

Figure 4.15 Interpretive processing panel showing the VSP-CDP transformed results for the far offset Ricinus VSP data resulting from the suggested "normal" runstream in chapter 2 (from Hinds et al., 1989a; Hinds et al., 1993c; Hinds et al., 1994c).

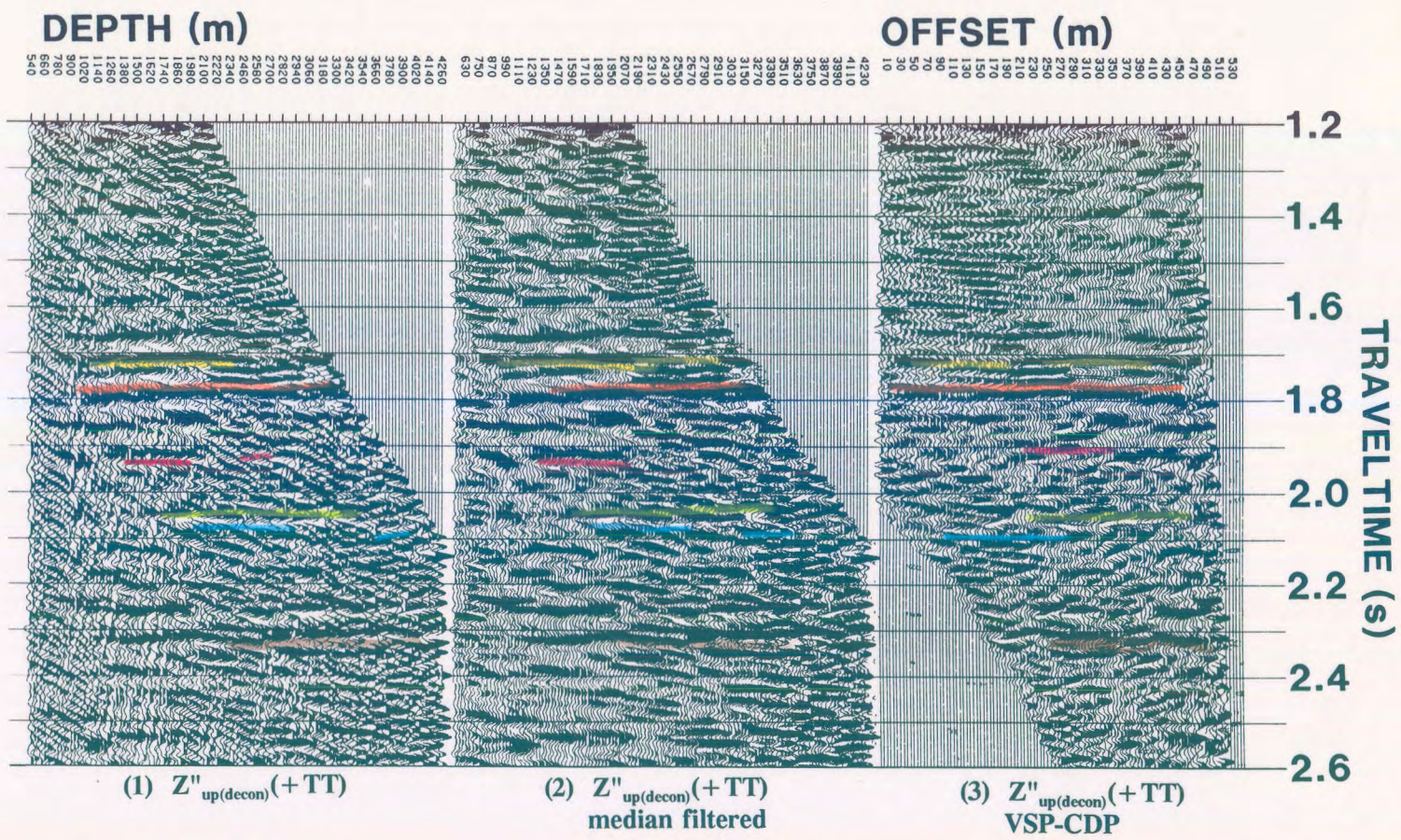

Figure 4.16 Interpretive processing panel showing the VSP-CDP transformed results for the deconvolved far offset Ricinus VSP data (from Hinds et al., 1993c; Hinds et al., 1994c).

4.6 Integrated interpretation

The integrated seismic display (ISD, see chapter 2) shows the surface seismic line merged with the VSP-CDP mapped results (panel 3 of Figure 4.14). The integrated seismic display in Figure 4.17 shows that the seismic interpretation displayed in Figure 4.3 extended the interpretation of the edge of the reef too far to the northeast, and supports the current interpretation as given in Figure 4.5.

These data also illustrate that the off-reef inter-Ireton event evident on the seismic section (Figure 4.5) extends about 500 m to the southwest. The surface seismic processing had sufficiently attenuated the SV events through the processing steps of normal moveout correction and CDP stacking. The interpretive processing enabled the desired attenuation of the SV events on the VSP data. The tie to the surface seismic up to 500 m away from the VSP well allows for the confident correlation of the inter-Ireton marker. Since only a small bundle of rays from the source to the well geophones has been affected by any Mesozoic faulting and the normal CDP summing found in surface seismic is not done in VSP processing, the coverage of the far offset VSP can be interpreted with a high level of confidence. By the processing that was applied in the rotations and the filtering which was evaluated using interpretive processing, the signal was enhanced enough to allow for an interpretation alongside the seismic data.

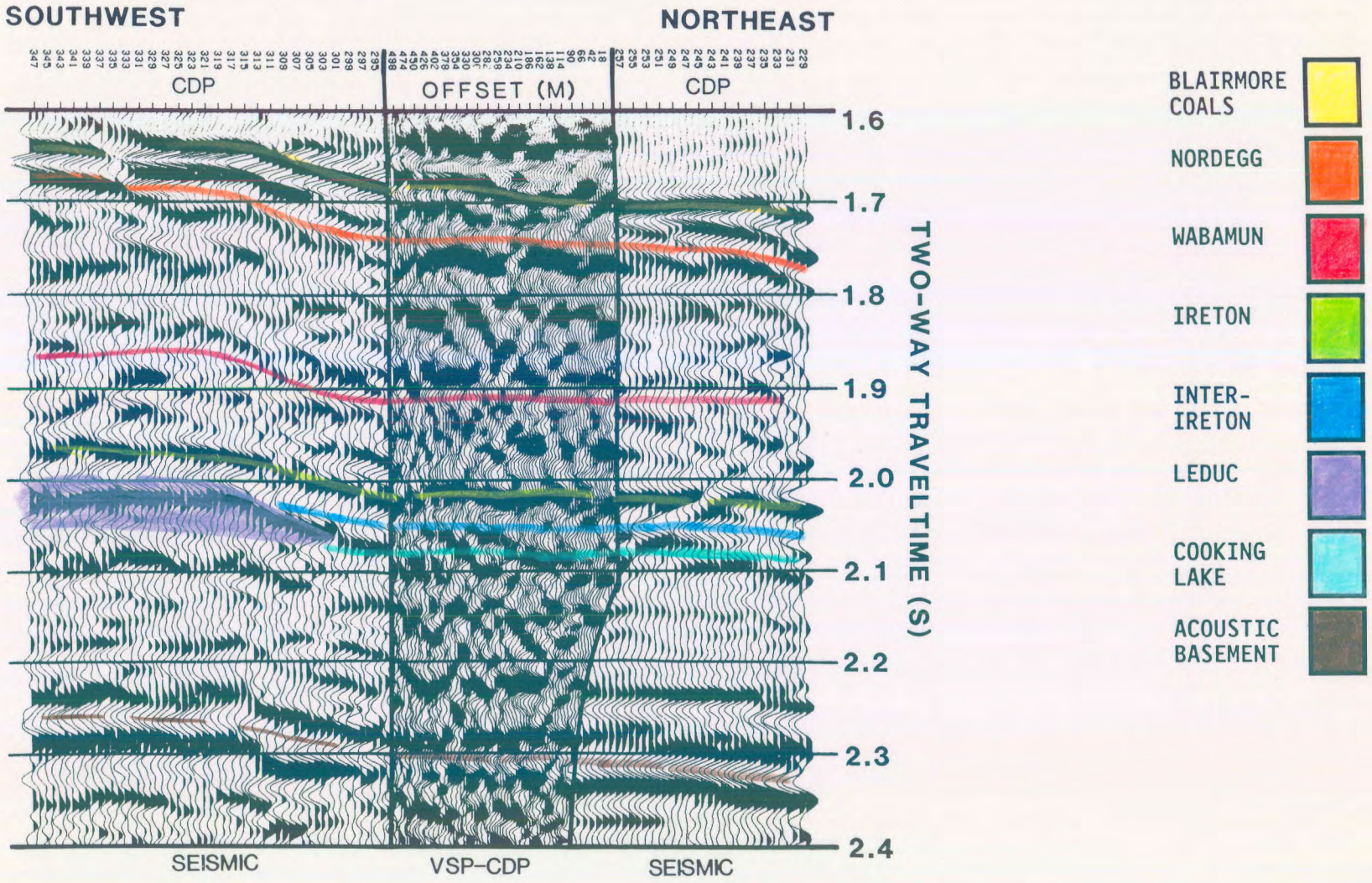

Figure 4.17 Integrated seismic display showing the VSP-CDP transformed far offset $Z''_{up}(+TT)$ data merged with the surface seismic data. These VSP data replace the surface seismic data at CDP's 258-293 (from Hinds et al., 1989a; Hinds et al., 1993c; Hinds et al., 1994c).

4.7 Interpretation discussion

The offsets for the Ricinus VSP survey were selected with the following considerations in mind:

1) If the atoll edge was in the near vicinity, then the inter-Ireton marker would terminate against the reef flank;

2) If the reef was further than 500 m (approximately half the 1100 m offset) away from the borehole or if the reef was in a different direction to the chosen offset direction, the inter-Ireton marker would be relatively flat and continuous;

3) the multiples that would affect a zero-offset seismic interpretation (migrated section) would be evident on the zero-offset VSP results; and

4) the exact geological tie with the seismic would be interpreted using the zero-offset VSP data.

The 199 m offset enabled an interpretation of the seismic signature at the well with a minimum of seismic interference from the complex Mesozoic faulting. The energy travelling down to the sonde in the borehole passes through the geological strata at near-normal incidence angles resulting in less ray bending than the CDP gathered surface seismic data. The well was in an off-reef position with the seismic interpretation being focused on the

Ireton, inter-Ireton, and Cooking Lake events rather than the Leduc event. The overlying marker that is used in isochron interpretation on the surface seismic was the Wabamun. The interpretational concern was that the Wabamun event was affected by the Blairmore coals or Nordegg multiples.

On the non-deconvolved near offset VSP data, interference with the Wabamun occurred until the geophone was below the Nordegg. The upgoing VSP events tied with the seismic section only after the VSP deconvolution was applied. The CDP stacking process within the surface seismic processing runstream enabled enough multiple attenuation to facilitate a Wabamun interpretation on the surface seismic data. The far offset VSP upgoing events did not critically require deconvolution (using the separated **HMAX'$_{down}$(-TT)** data to design the operator) and easily correlated to the surface seismic events.

The far offset VSP provided subsurface coverage for 500 m away from the VSP well site. Each trace represents approximately 6 m of subsurface coverage. The updated geological model based on the far offset VSP results is shown in Figure 4.4. In this figure, 6-9 and 7-15 are reefal; the VSP well however, is at least 500 m away from the reef edge.

The ISD in Figure 4.17 shows the seismic marker for the inter-Ireton within the range of the VSP-CDP coverage being continuous and displaying relatively little structure. Within the 500 m range away from the VSP well, the event does not terminate against the flank of the reef on the merged far offset VSP and seismic section. The Wabamun event in the far offset VSP data has not been affected appreciably by the multiples from the Blairmore coal zones due to the different geometry of the raypaths between the zero-offset VSP and the far offset

VSP. The Leduc reef event dips relatively steeply to the north of well 7-15 to the reefal platform position (Figs. 4.5 and 4.17) suggesting an abrupt edge may be present beyond 500 m southwest of the VSP well. The geological tie has been confidently interpreted from the IPP at the well location and the interpretation has been carried through to the merged far offset VSP and seismic dataset in the ISD, all using the philosophy of interpretive processing.

The mapping of the off-reef sediments enabled the final whipstock decision to be made. The decision was to abandon the well because the reef was more than 500 m away from the well location.